Repeated crustal thickening and recycling during the Andean orogeny in north Chile (21°–26°S)

M. Haschke[1]
Institut für Geologie, Geophysik und Geoinformatik, Freie Universität Berlin, Berlin, Germany

W. Siebel
Institut für Mineralogie, Petrologie und Geochemie, Universität Tübingen, Tübingen, Germany

A. Günther and E. Scheuber
Institut für Geologie, Geophysik und Geoinformatik, Freie Universität Berlin, Berlin, Germany

Received 1 June 2000; revised 9 January 2001; accepted 4 July 2001; published 29 January 2002.

[1] Understanding Neogene arc crustal thickening in the central Andes requires (1) some estimate of initial pre-Neogene (prior to 26 Ma) crustal thicknesses and (2) mechanisms that account for the remaining deficit in crustal thickening (10–30%). Mid-Miocene horizontal crustal shortening can explain most but not all crustal thickening in the modern central Andean arc. Systematic changes in geochemical and Sr, Nd, and selected Pb isotopic data of Late Cretaceous–Eocene (~78–37 Ma) and older arc magmatic episodes from north Chile provide new constraints on both. First, Andean crust may have been significantly thickened by long-term underplating of mantle-derived basalt from Jurassic to present. Second, estimated initial (late Eocene) crustal thicknesses of ~45 km are consistent with (1) amphibole- and garnet-bearing residual mineralogies for late Eocene syntectonic/posttectonic granitoids, (2) lower crustal *P* wave velocities of 7.3–7.7 km s^{-1} compatible with underplated mafic crust, and (3) results from recent experimental petrologic work showing garnet stability in mafic mineralogies ≥12 kbar (≥40 km crustal thickness). Analogous to older Andean magmatic episodes in north Chile, newly underplated basaltic crust may account for the remaining deficit in Neogene crustal thickening. Similar evolutionary patterns in geochemistry and initial Sr and Nd isotopic characteristics of Andean (200 Ma to present) magmatic rocks suggest that the Andean orogeny in this region evolved by a combination of processes of repeated arc migration, tectonic and magmatic crustal thickening, and igneous recycling which was controlled by periodically changing plate convergence rates and obliquity and corresponding changes in the rheologic behavior of the continental crust. *INDEX TERMS:* 1020 Geochemistry: Composition of the Crust, 1030 Geochemistry: Geochemical cycles (0330), 8159 Evolution of the Earth: Rheology–crust and lithosphere, 9360 Information Related to Geographic Region: South America; *KEYWORDS:* Andean Orogeny, Continental Crust, Recycling, Adakite, TTG, Crustal Thickening

1. Introduction

[2] Geochemical and isotopic variations of modern Andean magmatic arc rocks tend to correlate with changing crustal thicknesses through time in the central volcanic zone (CVZ) [e.g., *Kay et al.*, 1987, 1991, 1994; *Wörner et al.*, 1988, 1992, 1994; *Aitcheson et al.*, 1995; *McMillan et al.*, 1989, 1993; *Trumbull et al.*, 1999] and along the arc in the southern volcanic zone (SVZ) [*Hildreth and Moorbath*, 1988]. These correlations assume that melts equilibrated with and reflect the source mineralogy of a hydrous mafic melting assimilation storage homogenization (MASH) [*Hildreth and Moorbath*, 1988] crust-mantle boundary. Crustal thickening results in increasingly higher pressures for the residual mineralogy of melts produced from this source region. Geochemically, most diagnostic of pressure-induced changes in the source mineralogy, from lower-pressure assemblages dominated by plagioclase and clinopyroxene to higher-pressure amphibole and garnet-bearing mineral assemblages passing through the garnet stability field at depths ≥12 kbar or at crustal thicknesses ≥40 km, are rare earth elements (REEs), Y, Sr, Al_2O_3, and Na_2O [e.g., *Kay et al.*, 1987, 1991, 1994; *Drummond and Defant*, 1990; *Rushmer*, 1993; *Rapp and Watson*, 1995; *Petford and Atherton*, 1996]. The greatest chemical variations of this type occur where crust is thickest, i.e., the Western Cordillera and Altiplano-Puna plateau (up to 70 km [e.g., *James*, 1971; *Isacks*, 1988]). Although most of this crustal thickening can be explained by middle Miocene crustal shortening [*Isacks*, 1988; *Roeder*, 1988; *Sheffels*, 1990], still enigmatic is the remaining deficit in crustal thickening (10–30%) that could be attributed to magmatic addition or to an incorrect assessment of initial (prior to 26 Ma) crustal thickness [*Schmitz*, 1994; *Allmendinger et al.*, 1997]. The amount of material needed to fully balance crustal thickening is large (~20 km or ~500–800 km^3 km^{-1} m.y.$^{-1}$ during the last 15 m.y. [*Allmendinger et al.*, 1997], and most studies agree that simple magmatic addition by mantle-derived differentiates can only account for ~20–40 km^3 km^{-1} m.y.$^{-1}$ of the observed increase in crustal volume for the central Andes [*Reymer and Schubert*, 1984; *Francis and Hawkesworth*, 1994], insufficient to explain the entire Neogene crustal thickening.

[3] Constraints on both the missing crustal thickness and a mechanism for producing them, as well as estimates of crustal

[1]Now at Institut für Geowissenschaften, Universität Potsdam, Potsdam, Germany.

0148-0227/02/2001JB000328$09.00

thicknesses older than 26 Ma between 21° and 26°S come from older magmatic episodes. Since the beginning of subduction-related Andean magmatism some 200 m.y. ago, repeated stepwise eastward shifting of the main axis of arc magmatism generated a collage of four roughly parallel, eastward younging Andean magmatic arcs [*Coira et al.*, 1982; *Scheuber et al.*, 1994]: the Early Jurassic–Early Cretaceous arc along the present Coastal Cordillera, the Middle Cretaceous arc aligning with the Chilean Longitudinal Valley, the Late Cretaceous–Eocene arc largely corresponding to the Chilean Precordillera, and the late Oligocene–late Miocene arc and modern CVZ composing the Western Cordillera (Figure 1). Each set of arcs in this region is separated by up to 100-km-wide gaps with little or no magmatic rocks. These spatial and temporal variations make the north Chilean Andes an ideal site for studying long-term (~200 m.y.) crustal evolution and the timing of tectonic and magmatic processes at subduction-related noncollisional orogens.

[4] We compiled major and trace elements and isotopic data for these successive arcs and found similar evolutionary patterns in geochemistry with time. Each suite of arc magmatic rocks is characterized by systematically increasing La/Yb ratios and increasing Sr and Nd isotopic enrichment through time. Such patterns were neglected in previous studies owing to scarcity of data on rocks older than 26 Ma. Explaining the present anomalously thick crust in the central Andes requires that it must be viewed not just in terms of volumes and magnitudes but also in the light of its evolution [*Allmendinger et al.*, 1997]. In this paper, we discuss tectonic and magmatic data mainly from Late Cretaceous–Eocene magmatic rocks, as this paleoarc may hold the most important information on pre-Neogene (prior to 26 Ma) crustal thicknesses. Magmatic activity during this period occurred up to 100 km farther west of the modern volcanic front of the Western Cordillera, and deriving paleocrustal thicknesses from this arc is a reasonable but imperfect choice.

2. Database

[5] From the literature we compiled for petrogenetic evaluation major and trace elements and Sr and Nd isotopic data (501 samples) for Andean magmatic arc rocks (200 Ma to present) in addition to analytical work by *Haschke* [1999]. Data for Jurassic–Early Cretaceous rocks (104 samples) come from the work of *Rogers and Hawkesworth* [1989], *Lucassen and Franz* [1994], and *Kramer et al.* [1998]; for Middle Cretaceous rocks (29 samples), data come from *Lucassen and Franz* [1994], for Late Cretaceous–late Eocene rocks (171 samples), data come from *Rogers and Hawkesworth* [1989], *Maksaev* [1990], *Döbel et al.* [1992], *Williams* [1992], *Heumann et al.* [1993], and *Pichowiak* [1994], and for late Oligocene to present magmatic rocks (197 samples), data come from *Kay et al.* [1987, 1991, 1994], *Wörner et al.* [1988, 1994], and *Trumbull et al.* [1999]. We also present 65 new analyses of volcanic and intrusive rocks with ages between 78 and 37 Ma, published by *Haschke* [1999], to fill spatial and temporal gaps from earlier work and to establish pre-Neogene crustal thicknesses. Correlating age data are from *Mpodozis et al.* [1993] and 17 new K/Ar ages are from *Haschke* [1999]. Sample locations and representative new analyses are listed in Tables 1–6. The complete database is available upon request from M. Haschke.

3. Tectonomagmatic Setting and History of Late Cretaceous–Eocene Magmatic Rocks in North Chile

[6] The magmatic and tectonic evolution of the Late Cretaceous–Eocene arc in north Chile has been influenced by changes in plate convergence rates, convergence obliquity [*Pardo-Casas and Molnar*, 1987; *Somoza*, 1998], and dip of the subducting plate [*Haschke et al.*, 2001]. During this period the rate of plate convergence more than doubles (from <5 to >10 cm yr^{-1} [*Pardo-Casas and Molnar*, 1987]), substantially decreasing arc-normal obliquity. The highly oblique subduction and low convergence rates in the Late Cretaceous correlated with intra-arc and back arc extension and back arc alkaline magmatism [*Scheuber et al.*, 1994], whereas nearly arc-normal Eocene subduction at high convergence rates corresponded to transpression, followed by shortening and thickening of the crust (14.5% [*Günther et al.*, 1998]). Since the change in convergence parameters occurred at ~49 Ma [*Pardo-Casas and Molnar*, 1987], most of the Late Cretaceous–Eocene magmatic activity occurred in an extensional tectonic arc and back arc setting (up to 44 Ma [*Scheuber et al.*, 1994; *Charrier and Reutter*, 1994]).

[7] Like other continental arcs (e.g., Andean SVZ [*Hickey et al.*, 1986]), the composition of magmatic rocks from this period ranges from calc-alkaline basaltic andesite to rhyolite (and intrusive equivalents) but is dominated by intermediate and silicic compositions. During Late Cretaceous times, more mafic alkaline magmatism occurred in the transition from the arc to back arc regime where alkaline plutons (Cerro Quimal at 66.4 Ma and Cerro Colorado at 66.6 Ma [*Maksaev*, 1990]) intrude up to 4000-m-thick Late Cretaceous continental red beds along N-S trending horst-and-graben structures [*Charrier and Reutter*, 1994]. These relations between Late Cretaceous alkaline magmatism and rift-related faulting indicate an incipient back arc rifting regime during this time.

[8] Magmatic rocks produced during the period of increasing convergence rates and decreasing convergence obliquity (~49 Ma [*Pardo-Casas and Molnar*, 1987]) are rare and are represented mostly by mafic dikes ranging in age from 49.5 [*Haschke*, 1999] to 45.4 Ma [*Döbel et al.*, 1992]. Following the increased convergence rates, calc-alkaline arc magmatism continued into the middle to late Eocene, and minor mafic to intermediate calc-alkaline monogenetic centers (Cerro Negro at 40.2 ± 1.6 Ma [*Haschke*, 1999]; Cerro Olivino at 40.8 ± 1.4 Ma [*Mpodozis et al.*, 1993]) occur along strike of the NW-SE trending Calama-Olacapato-El Toro fracture zone across the arc. This fracture zone might have served as a pathway for less differentiated melts prior to Incaic crustal shortening, as younger (late Miocene–Pliocene), glassy mafic andesitic to andesitic syntectonic/posttectonic flows also occur along fault zones in the Maricunga belt in north Chile [*Kay et al.*, 1994].

[9] The youngest magmatic rocks of this arc are mainly granodiorites and granites from the El Abra-Fortuna batholith (39–37 Ma [*Dilles et al.*, 1997]), which intrude into older middle to late Eocene portions of this pluton. They were produced coeval and subsequent to Incaic transpressional deformation (38.5 Ma [*Döbel et al.*, 1992]) before arc magmatic activity ceased. Arc magmatism during this period must have created considerable relief between the arc and back arc region, where >3000 m of conglomerates were deposited [*Charrier and Reutter*, 1994].

[10] Magmatic activity resumed at ~26 Ma in the Western Cordillera [*Kay et al.*, 1994] after a period of relative magmatic quiescence lasting ~10 m.y. These changes in temporal and spatial magmatic patterns argue for substantial changes in subduction geometry possibly caused by a period of flat subduction similar to the one inferred for the present-day flat slab region [*Isacks*, 1988; *Kay et al.*, 1991; *Haschke et al.*, 2001]. Evidence for subduction erosion comes from progressive eastward younging of magmatic rocks (Figure 1, inset) and the overall lack of Mesozoic forearc rocks of the leading edge of South America [*Rutland*, 1971; *von Huene and Scholl*, 1991].

[11] Our structural and magmatic analyses show that the Andean evolution prior to 26 Ma was characterized by (1) eastward

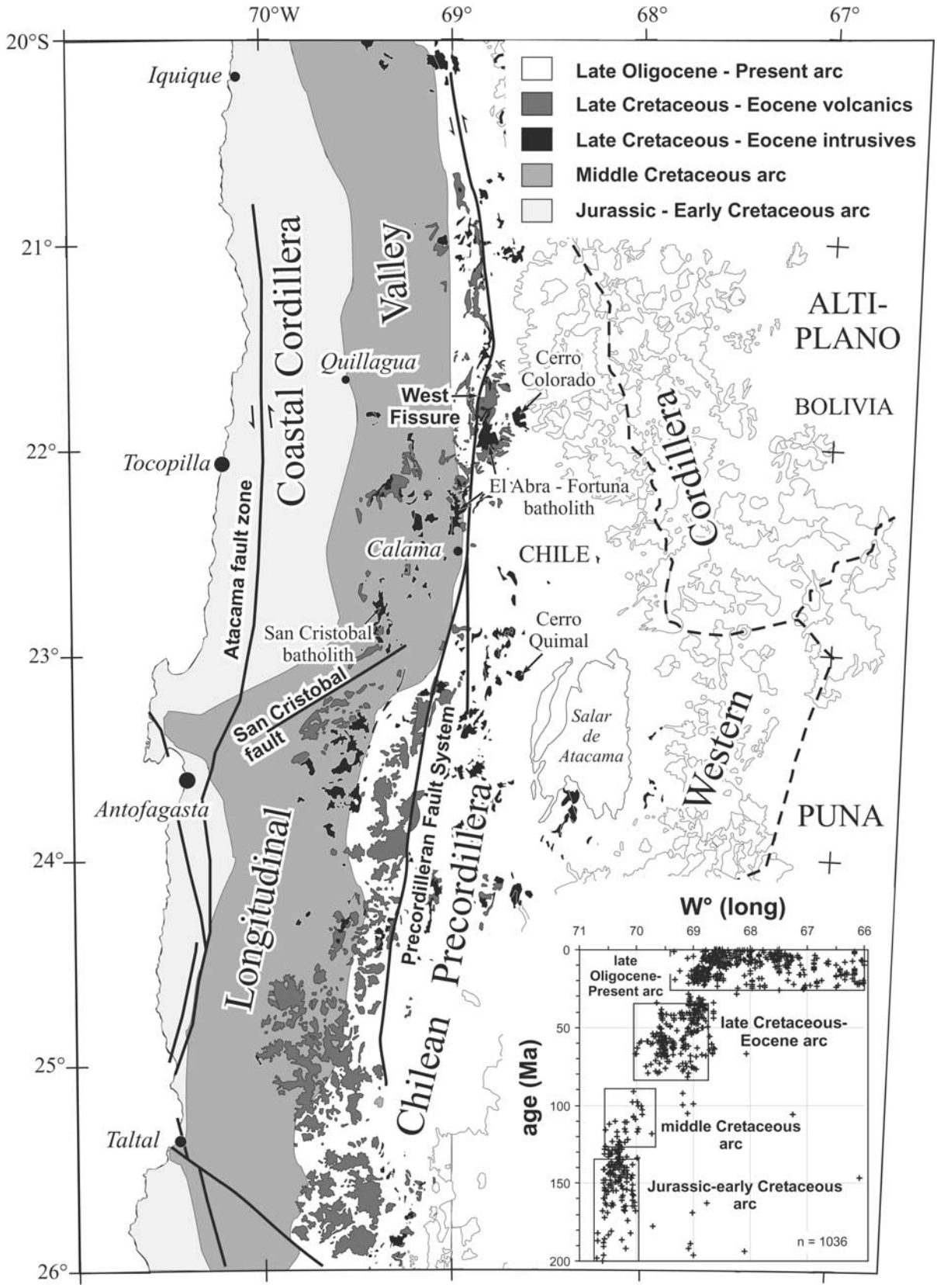

Figure 1. Simplified geologic map of the Andes in northern Chile, schematically showing distribution of pre-Neogene and modern volcanic rocks in the central Andes. Solid lines mark trench-linked strike-slip fault zones in each arc. Inset shows plot of age (Ma) of Andean magmatic rocks of the northern central Andes versus longitude (°W).

Table 1. Geochemical Analyses of Representative Late Cretaceous–Eocene Samples From This Study, 78–63 Ma Arc[a]

	NN-AA3	SS-G2	SS-K2	3L-C9	SS-K1c	SS-D8	SS-F2 (1)	SS-F2 (2)	SS-D9	SS-B4	SS-i2a
Longitude, °W	69.242	69.715	68.965	69.349	69.041	69.951	69.952	69.952	70.036	69.489	69.428
Latitude, °S	22.130	24.562	22.931	22.454	23.092	24.897	24.703	24.703	24.928	24.939	23.904
Age, Ma				67.5 ± 2.3							
Type	lava	lava	lava	lava	tuff	lava	ignimbrite	ignimbrite	lava	lava	tuff
SiO_2	53.19	58.68	59.97	60.81	69.73	74.44	74.54	–	74.94	75.63	76.09
TiO_2	1.00	1.05	1.03	0.70	0.88	0.21	0.15	–	0.19	0.21	0.15
Al_2O_3	18.27	19.32	16.62	17.81	13.60	13.56	13.12	–	13.46	13.23	12.41
FeO*	7.69	5.90	6.48	5.13	4.58	1.40	1.38	–	1.54	1.70	0.80
MnO	0.14	0.11	0.10	0.14	0.03	0.02	0.05	–	0.02	0.04	0.04
MgO	4.77	1.95	1.44	3.46	0.37	0.84	0.41	–	0.38	0.50	0.44
CaO	8.64	6.66	6.14	2.61	1.76	1.44	1.19	–	1.20	1.30	0.47
Na_2O	3.92	3.73	4.00	6.50	3.63	2.45	3.21	–	3.81	3.34	4.70
K_2O	1.33	1.73	3.24	2.08	4.70	5.45	5.74	–	4.28	3.83	4.80
P_2O_5	0.18	0.21	0.26	0.18	0.22	0.03	0.05	–	0.01	0.05	0.02
Total	99.14	99.34	99.28	99.43	99.49	99.84	99.84	–	99.83	99.81	99.91
LOI	4.88	1.23	2.70	2.61	1.75	1.47	0.90	–	0.62	1.03	2.16
La	18.2	21.2	35.1	15.2	38.9	24.6	34.6	32.9	25.9	26.9	30.5
Ce	40.7	49.9	74.2	32	94.5	53.8	66	60	54.4	54.3	66.6
Nd	23.4	25.1	34.5	15	37.7	20.5	26.0	25.0	19.7	21.8	24.2
Sm	5.20	6.15	7.26	3.36	10.40	4.20	4.56	4.41	3.86	4.18	4.61
Eu	1.31	1.60	1.53	0.95	1.41	0.56	0.36	0.39	0.36	0.42	0.42
Tb	0.755	0.900	0.999	0.5	1.198	0.559	0.7	0.7	0.448	0.518	0.540
Y	18	24	28	9	44	39	34	34	32	32	37
Yb	2.54	3.07	3.34	1.4	4.87	2.43	3.5	3.4	2.20	2.44	2.62
Lu	0.379	0.477	0.497	0.2	0.763	0.391	0.6	0.5	0.344	0.370	0.382
Rb	19	42	99	46	168	243	229	234	194	159	178
Sr	452	354	467	523	243	150	69	69	92	156	53
Ba	358	304	693	832	1827	535	354	351	541	646	556
Pb	5	12	9	12	22	15	22	22	20	20	26
Cs	3.98	4.42	3.52	15.5	5.03	8.42	12.1	11.8	6.62	4.61	2.00
U	1.00	1.38	4.06	1.0	6.30	3.77	3.1	3.2	2.90	3.44	3.80
Th	4.19	5.85	14.13	3.2	26.09	23.82	21.9	21.5	18.68	15.56	19.63
Zr	104	134	197	134	443	154	135	135	140	134	120
Hf	3.46	4.46	6.45	3.6	13.52	4.32	4.4	4.2	4.06	4.14	3.55
Nb	6	9	14	7	20	10	10	10	13	13	26
Ta	0.40	0.66	1.22	4.0	1.62	0.79	0.9	1.1	1.03	0.87	1.78
Sc	26.3	22.1	18.8	13.79	15.7	3.9	3.83	3.70	3.6	4.7	2.4
Cr	38.3	5.8	11.8	31.9	ND	1.2	6.8	7.3	ND	ND	0.4
Ni	14	2.8	2	10	1.3	ND	1	1	0.3	0.9	0.2
Co	30.7	11.5	17.7	17.1	3.4	1.5	2.3	2.3	1.6	2.0	0.5
V	168	104	123	110	53	36	31	31	30	24	22
$^{87}Sr/^{86}Sr$					0.707185				0.709867		
$^{87}Sr/^{86}Sr$ i					0.705117				0.703858		
$^{143}Nd/^{144}Nd$					0.512744				0.512706		
$^{143}Nd/^{144}Nd$ i					0.512756				0.512739		
eNd					2.30				1.97		
$^{206}Pb/^{204}Pb$					18.695				18.744		
$^{206}Pb/^{204}Pb$ i					18.430				18.567		
$^{207}Pb/^{204}Pb$					15.639				15.629		
$^{207}Pb/^{204}Pb$ i					15.626				15.621		
$^{208}Pb/^{204}Pb$					38.795				38.792		
$^{208}Pb/^{204}Pb$ i					38.443				38.428		

[a] Analytical standards and techniques are as those of *Kay et al.* [1987]; ND indicates not determined.

migration of the arc, (2) repeated changes between flat slab and steeper slab subduction and associated changes between compressive (thickening) and extensional (thinning) regimes, and (3) tectonic erosion of the leading edge of the upper plate. We will now explore the correlation between the tectonic evolution and changing composition of associated magmatism.

4. Geochemistry of Late Cretaceous–Eocene Magmatic Rocks in North Chile

4.1. Major and Trace Elements

[12] Overall, the geochemistry of Late Cretaceous–Eocene magmatic rocks in north Chile is characterized by three distinct magmatic suites: (1) a larger-volume calc-alkaline suite of medium- to high-K pyroxene and/or amphibole-bearing basaltic andesites to dacites and rhyolites, (2) a smaller volume of a more alkaline back arc suite of gabbros to granodiorites, and (3) scattered calc-alkaline mafic andesitic centers aligned along fracture zones near Calama. As is typical for most CVZ and SVZ arc volcanic rocks, the high Ba/Nb ratios (>30) of Late Cretaceous–Eocene rocks from both the calc-alkaline and alkaline magmatic suites are consistent with melts produced in a metasomatized mantle wedge above a dehydrating subducting slab [e.g., *Hildreth and Moorbath*, 1988; *Kay et al.*, 1991].

[13] The most mafic rocks of the Late Cretaceous–Eocene main arc front are typical basaltic andesites with characteristically

Table 2. Geochemical Analyses of Representative Late Cretaceous–Eocene Samples From This Study, 78–63 Ma Back Arc

	NN-A1b	XR88-101	XR88-100b	XR88-98
Longitude, °W	68.655	68.672	68.672	68.672
Latitude, °S	21.889	23.108	23.108	23.108
Age, Ma				
Type	intrusion	intrusion	intrusion	intrusion
SiO_2	57.41	50.30	50.53	52.85
TiO_2	1.06	0.93	0.80	0.84
Al_2O_3	18.32	18.34	17.13	19.23
FeO*	1.95	8.86	7.36	6.43
MnO	0.13	0.30	0.19	0.20
MgO	3.00	3.09	5.75	2.01
CaO	9.96	7.85	7.20	6.73
Na_2O	4.62	2.73	5.06	4.53
K_2O	2.77	5.99	4.39	6.02
P_2O_5	0.53	0.62	0.75	0.45
Total	99.75	99.01	99.17	99.29
LOI	0.46	0.25	0.58	0.16
La	28.4	38.2	31.8	35.3
Ce	68.7	78	62	70
Nd	36.9	41	31	33
Sm	7.18	8.91	6.05	6.96
Eu	1.58	2.71	2.03	2.41
Tb	0.920	0.9	0.8	0.8
Y	24	25	24	26
Yb	3.16	2.6	2.0	2.0
Lu	0.461	0.4	0.3	0.3
Rb	45	123	153	170
Sr	1226	1851	1391	1945
Ba	805	1419	1342	1250
Pb	17	13	15	11
Cs	1.28	2.8	2.9	2.9
U	2.45	1.7	2.4	1.1
Th	7.43	6.3	6.5	3.6
Zr	101	143	155	100
Hf	3.29	5.1	4.3	3.1
Nb	16	12	14	9
Ta	0.79	0.7	0.9	0.5
Sc	18.2	16.84	16.87	10.71
Cr	2.4	8.9	134.2	11.6
Ni	2.0	3	82	46
Co	10.2	24.6	25.9	16.1
V	113	230	183	170
$^{87}Sr/^{86}Sr$	0.704774			
$^{87}Sr/^{86}Sr$ i	0.704648			
$^{143}Nd/^{144}Nd$	0.512769			
$^{143}Nd/^{144}Nd$ i	0.512803			
eNd	3.21			
$^{206}Pb/^{204}Pb$	18.650			
$^{206}Pb/^{204}Pb$ i	18.517			
$^{207}Pb/^{204}Pb$	15.638			
$^{207}Pb/^{204}Pb$ i	15.632			
$^{208}Pb/^{204}Pb$	38.666			
$^{208}Pb/^{204}Pb$ i	38.536			

high alumina (Al_2O_3 18–19.6 wt %), low MgO (<5 wt %), Ni (<30 ppm), and Cr (<100 ppm) contents. Their most common phenocrysts are calcic plagioclase (bytownite to andesine) and clinopyroxene along with plagioclase microphenocrysts; olivine is rare. Primitive basalts are unknown anywhere along the arc but occur locally in the back arc in Bolivia and northern Chile as rift-related picritic alkaline flows (G. Wörner, personal communication, 1999). The alkaline gabbros from the arc to back arc transition show slightly higher MgO (<6 wt %), Ni (up to 82 ppm), and Cr (up to 134 ppm) concentrations, and mafic rocks from the monogenetic centers show slightly lower MgO (<4 wt %) contents relative to mafic main arc rocks but still much lower MgO contents compared to primitive mantel basalts, too low for equilibration with peridotite.

[14] Late Cretaceous–Eocene basaltic andesites (52–57 wt % SiO_2) show fractionated but largely overlapping REE patterns through time (Figure 2a) with small negative Eu anomalies (Eu/Eu* 0.8–0.9). Evolution of La/Yb and Sr/Y ratios of these rocks shows a slight increase (La/Yb from 5–7 to 11–16 and Sr/Y from <25 to >40). This evolution is mainly due to gradually decreasing Yb (from 2.1–2.5 to 1.4–2.4 ppm) and Y (from 18–36 to 14–24 ppm) concentrations and increasing Sr contents (from 400–500 to 700–900 ppm). Late Eocene syntectonic/posttectonic basaltic andesites are not known from this region.

[15] The alkaline mafic diorites (78–63 Ma) in the arc to back arc transition are characterized by light REE-enriched patterns (Figure 2a) with lack of or small positive Eu anomalies (Eu/Eu* 1.0–1.1) and higher La/Yb (11–16) and Sr/Y (>50) ratios. One explanation for such characteristics may be decreasing degrees of asthenospheric partial melting due to diminishing slab dehydration ~100 km east of the main arc magmatic front. This is consistent with the overall large-ion lithophile element (LILE) and high field strength element (HFSE) enriched signatures of these rocks [*Haschke*, 1999]. Extreme enrichment of these elements in rocks from the monogenetic centers suggests that they might have formed at even lower degrees of partial melting.

[16] Intermediate and silicic arc volcanic and intrusive rocks from this period show progressive compositional variations with increasing SiO_2 and decreasing age, such that the largest chemical contrast occurs between the oldest (Late Cretaceous) and the youngest (late Eocene) dacitic (and granodioritic) and rhyolitic (and granitic) rocks (Figure 2, see insets). Intermediate–Late Cretaceous to middle to late Eocene main arc compositions (57–63 wt % SiO_2) show more fractionated, overlapping REE patterns (Figure 2b) with larger negative Eu anomalies (Eu/Eu* of 0.6–0.9) than mafic andesites but slightly steeper, heavy REE patterns with decreasing age. Most andesites of this period are characterized by increasing La/Yb (from 5–7 to 14–26) and Sr/Y ratios (from 5–20 to 30–60) through time because of decreasing Yb (from 2.5–3.7 to 1.1–1.9 ppm) and Y (from 24–32 to 13–20 ppm) and increasing Sr contents (350–470 to 530–920 ppm) with decreasing age. Late Eocene syntectonic/posttectonic andesitic eruptions are present as thin ash layers in continental sediments of the Sichal formation [*Döbel et al.*, 1992].

[17] Late Cretaceous to middle to late Eocene main arc dacitic and granodioritic compositions (63–68 wt % SiO_2) exhibit fractionated REE patterns (Figure 2c) with systematically steeper, heavy REE patterns and decreasing negative Eu anomalies with decreasing age (Eu/Eu* from 0.5–0.7 to 0.6–1.0). La/Yb and Sr/Y values of these rocks increase through time from mostly low La/Yb (6–9) and Sr/Y (<20) ratios to higher La/Yb (12–17) and Sr/Y (15–45) ratios in middle to late Eocene. Younger (late Eocene) syntectonic/posttectonic granodiorites have the highest La/Yb (18–27) and Sr/Y (28–69) ratios among dacitic and granodioritic compositions from this period. Responsible for this La/Yb and Sr/Y evolution between Late Cretaceous to mid–late Eocene dacites and granodiorites are progressively decreasing Yb (from 5.9 to 0.8 ppm) and Y (from 57 to 10 ppm) concentrations and increasing Sr contents (from mostly 250–350 to 330–670 ppm).

[18] Late Cretaceous–Eocene rhyolitic and granitic rocks (>68 wt % SiO_2) show extremely fractionated REE patterns (Figure 2d) with strongly steepening, heavy REE patterns with decreasing age and decreasing negative Eu anomalies (Eu/Eu* from 0.2–0.4 to 0.8). The oldest rhyolites show mainly low La/Yb (7–12) and Sr/Y (1–6) ratios, progressively increasing to higher ratios of La/Yb (11–25) and Sr/Y (4–77) in middle to late Eocene. Late

Table 3. Geochemical Analyses of Representative Late Cretaceous–Eocene Samples From This Study, 63–52 Ma Arc

	NN-O5	S-A3 (1)	S-A3 (2)	SS-i3	NN-T9	NN-Q1a	NN-P3	SS-J3	NN-P7	SS-D5	NN-P2	SS-H1	SS-E1	SS-G6	SS-A1	SS-C7	NN-T8	NN-Q1b	N-E2	SS-A9
Longitude, °W	69.055	69.143	69.143	69.357	69.007	69.103	68.954	69.214	68.95	69.864	68.969	69.354	69.812	69.466	69.619	69.627	68.979	69.102	68.98	69.64
Latitude, °S	22.064	23.078	23.078	23.7	21.939	22.303	22.085	23.21	22.074	24.886	22.105	24.235	25.802	24.365	25.699	24.801	21.929	22.302	21.832	25.465
Age, Ma	52.9 ± 1.8	60.8 ± 1.6			53.5 ± 2.2				52.6 ± 1.8									50.8 ± 1.3		
Type	lava	lava	lava	lava	lava	intrusion	lava	lava	lava	lava	lava	lava	lava	lava	lava	lava	lava	lava	tuff	lava
SiO_2	56.06	52.61	–	52.82	55.72	56.20	57.24	57.05	58.87	59.07	60.50	61.24	61.54	61.74	62.35	62.77	62.97	68.07	68.87	65.02
TiO_2	0.81	1.13	–	0.89	0.94	1.10	0.97	0.93	0.87	0.80	0.99	0.71	0.78	1.02	0.84	0.77	0.63	0.51	0.51	0.82
Al_2O_3	17.93	18.14	–	18.83	19.35	17.51	17.36	18.16	16.75	16.53	18.59	17.35	16.92	17.39	17.09	17.09	17.41	16.50	15.58	17.26
FeO*	6.06	8.80	–	7.54	6.97	6.77	6.24	6.01	6.03	5.85	4.83	5.21	5.08	4.78	4.80	5.14	5.07	2.75	3.87	3.91
MnO	0.12	0.16	–	0.13	0.14	0.12	0.11	0.10	0.10	0.11	0.09	0.10	0.09	0.09	0.05	0.16	0.12	0.05	0.15	0.06
MgO	3.14	5.00	–	4.72	3.11	4.10	3.66	3.34	3.79	3.60	2.09	3.21	2.84	2.18	2.09	1.83	1.56	1.69	0.35	0.93
CaO	7.74	8.47	–	9.68	7.68	6.96	6.45	6.92	6.36	6.86	3.86	5.07	5.15	4.22	4.63	4.73	5.10	2.81	3.90	3.91
Na_2O	3.45	3.12	–	3.20	4.49	3.72	4.21	4.16	3.65	3.74	5.14	3.75	4.07	4.94	4.43	4.04	4.18	3.92	4.21	4.60
K_2O	3.62	1.38	–	1.16	0.53	2.50	2.63	2.23	2.66	2.47	3.05	2.60	2.78	2.80	2.98	2.72	2.13	3.25	1.95	2.78
P_2O_5	0.39	0.22	–	0.18	0.30	0.27	0.44	0.41	0.25	0.31	0.32	0.18	0.19	0.31	0.22	0.17	0.26	0.16	0.18	0.27
Total	99.33	99.02	–	99.16	99.23	99.25	99.30	99.33	99.33	99.35	99.46	99.42	99.43	99.47	99.47	99.43	99.43	99.69	99.57	99.57
LOI	1.50	1.34	–	0.29	1.22	0.49	1.06	1.60	1.85	0.88	2.04	1.23	0.84	1.64	0.79	0.79	0.58	2.45	0.66	1.26
La	66.5	15.3	16.5	16.3	25.0	28.7	45.7	26.5	32.0	21.7	32.5	21.1	23.3	33.1	33.2	21.7	27.3	23.0	28.3	30.9
Ce	135.5	29	35	35.8	49	61.9	94.5	57.9	67.1	45.2	70.4	48.3	52.3	71.6	72.0	47.3	58.8	47.7	53	70.2
Nd	65.4	18.0	19	16.5	28	27.5	48.3	26.4	32.6	18.8	37.5	18.5	24.7	30.4	30.0	22.7	26.9	21.9	27	33.2
Sm	11.22	4.66	4.46	3.87	5.60	5.80	8.13	5.61	6.27	4.53	7.36	4.81	5.20	6.29	6.46	4.66	5.45	3.90	4.92	7.40
Eu	2.39	1.12	1.65	1.12	1.65	1.33	1.78	1.50	1.50	1.22	1.62	1.12	1.06	1.41	1.33	0.94	1.17	0.82	1.34	1.61
Tb	0.856	0.699	0.6	0.549	0.7	0.679	0.715	0.629	0.633	0.596	0.852	1.004	0.461	0.757	0.731	0.536	0.687	0.315	0.5	0.929
Y	22	16	16	15	20	22	19	18	19	18	26	21	22	24	24	22	21	19	20	32
Yb	2.32	2.35	2.3	1.76	2.4	1.85	1.73	1.95	1.83	1.60	2.88	1.89	1.65	2.27	2.34	2.08	2.36	0.68	2.10	2.98
Lu	0.311	0.363	0.3	0.264	0.4	0.281	0.251	0.295	0.263	0.220	0.414	0.295	0.226	0.326	0.349	0.312	0.360	0.088	0.3	0.438
Rb	50	38	31	23	4	92	42	39	54	70	69	76	98	73	82	86	57	102	62	125
Sr	1938	437	437	778	620	646	1341	902	713	775	631	559	562	506	477	459	538	537	452	396
Ba	1085	385	361	285	432	482	1084	1591	846	743	768	628	686	689	750	583	723	698	641	688
Pb	5	2	2	3	9	19	8	19	8	11	11	8	15	13	16	14	7	14	10	15
Cs	0.40	5.29	6.0	0.66	0.8	10.11	0.56	6.96	1.27	3.47	1.33	2.19	5.87	4.56	1.89	3.68	2.14	7.29	1.0	6.18
U	5.24	0.74	0.8	1.30	0.8	4.28	2.65	1.47	2.50	2.16	1.89	3.48	3.65	3.32	3.38	3.30	1.68	1.88	1.1	3.35
Th	15.05	2.01	2.4	4.41	3.6	12.32	9.49	4.56	8.51	6.34	6.83	12.22	12.82	10.53	10.59	10.30	5.44	6.24	3.9	12.40
Zr	130	98	98	84	170	112	132	140	136	121	190	137	172	217	218	134	176	146	178	239
Hf	4.64	2.99	3.3	2.90	5.3	4.12	4.35	4.45	4.44	3.93	5.43	4.60	5.38	5.84	6.35	3.88	4.87	3.87	4.7	6.90
Nb	8	7	7	5	7	9	11	9	9	8	13	9	8	16	13	8	11	8	13	15
Ta	0.46	0.42	0.42	0.30	0.5	0.62	0.62	0.65	0.71	0.52	0.78	0.70	0.66	1.06	0.86	0.66	0.70	0.44	0.5	1.05
Sc	14.4	26.3	28.89	26.6	14.37	17.8	12.1	15.1	17.8	16.9	14.2	14.1	12.4	12.3	12.0	11.7	7.5	4.7	5.72	10.4
Cr	4.5	35.5	41.3	98.3	13.1	38.3	4.4	19.6	65.3	36.1	nd	14.2	39.1	2.4	5.5	nd	nd	3.5	15.5	1.4
Ni	7	33.6	33.6	98.3	2	16	8	12	14	8	3.2	7	15	2	5	2	3.4	4.8	4	2.6
Co	14.9	31.5	32.0	34.0	17.1	22.6	17.0	18.4	20.5	19.6	9.3	16.7	17.5	9.8	12.7	14.8	9.9	6.4	6.5	13.3
V	135	212	212	175	132	165	145	131	150	123	105	118	99	103	109	117	71	59	54	75
$^{87}Sr/^{86}Sr$	0.704214							0.704376	0.706605				0.704490					0.705259		
$^{87}Sr/^{86}Sr$ i	0.704148							0.704270	0.706434				0.704021					0.704954		
$^{143}Nd/^{144}Nd$	0.512823							0.512713	0.512710				0.512792					0.512685		
$^{143}Nd/^{144}Nd$ i	0.512855							0.512736	0.512737				0.512818					0.512706		
eNd	4.23							1.92	1.93				3.51					1.33		
$^{206}Pb/^{204}Pb$	18.824							18.546	18.698				18.621					18.668		
$^{206}Pb/^{204}Pb$ i	18.398							18.486	18.489				18.375					18.589		
$^{207}Pb/^{204}Pb$	15.599							15.602	15.613				15.618					15.626		
$^{207}Pb/^{204}Pb$ i	15.579							15.599	15.603				15.606					15.622		
$^{208}Pb/^{204}Pb$	38.704							38.534	38.662				38.644					38.652		
$^{208}Pb/^{204}Pb$ i	38.312							38.474	38.434				38.367					38.567		

Eocene syntectonic/posttectonic granites have the highest La/Yb (19–34) and Sr/Y ratios (19–54) among rhyolitic/granitic compositions. These systematic changes are due to progressively decreasing Yb (from 2.2–4.2 to 1.3–1.5 ppm) and Y (from 21–49 to 17–30 ppm) and increasing Sr contents (from mostly 53–156 to >300 ppm) with decreasing age. Still lower Yb (0.6–0.7 ppm) and Y (8–16 ppm) and higher Sr concentrations (224–634 ppm) account for the higher La/Yb and Sr/Y ratios of the syntectonic/posttectonic granites.

[19] Parallel to these changes in trace element composition are progressively increasing Al_2O_3 and Na_2O contents between Late Cretaceous and late Eocene; in dacites and granodiorites, Al_2O_3 increases from 15.8 to 17.0 wt % and Na_2O increases from 4.0 to 4.5 wt %, and in rhyolites and granites, Al_2O_3 increases from 12.7 to 15.6 wt % and Na_2O increases from 3.3 to 4.1 wt %.

[20] Many of these characteristics of the youngest (late Eocene) dacites-granodiorites and rhyolites-granites match those of adakites (i.e., primary dacitic melts from subducting oceanic crust [*Stern et al.*, 1984; *Drummond and Defant*, 1990; *Peacock et al.*, 1994]) and of partial melts from newly underplated basaltic crust [*Atherton and Petford*, 1993; *Petford and Atherton*, 1996]. Both petrogenetic models attribute the distinct geochemical signatures of the silicic rocks to partial melting of garnet and/or amphibole-bearing (hydrous) basaltic crust; the more silicic (rhyolitic-granitic) melts may reflect lower degrees of partial melting than those generating the dacites [*Rapp and Watson*, 1995]. The slab-melting model is attractive with respect to the genesis of the syntectonic/posttectonic El Abra-Fortuna granitoids, as subduction has been a major feature of the Andean continental margin since at least the Jurassic, and the rocks have characteristics similar to slab melts. However, geophysical, geologic, isotopic, and age data from our study suggest that partial melting of a mafic base of thick orogenic crust (>40 km) beneath the batholith is more likely (see discussion by *Atherton and Petford* [1993] and *Petford and Atherton* [1996]). The late Eocene syntectonic/posttectonic El Abra-Fortuna batholith overlies the newly thickened, late Eocene crustal keel of the Andes, here ~45 km thick.

[21] Increasing proportions of residual amphibole and garnet produce melts with steep, heavy REE patterns since garnet preferentially retains the heavy REEs and Y, leading to high La/Yb and Sr/Y ratios in low-degree partial melts. Retention of amphibole in the source region, or its subsequent fractionation during lower-pressure differentiation, can also steepen REE patterns, but without garnet, even extreme amphibole fractionation results in La/Yb ratios only as high as 14–15 and middle REE-depleted (Gd to Er) concave upward REE patterns [*Kay et al.*, 1989]. Particularly diagnostic for increasing hydrous melting are the high La/Yb and Sr/Y ratios and the decreasing negative Eu anomalies of the silicic rocks, as they indicate increasing meltwater fugacity (f_{H2O}) through dehydration melting of amphibole-bearing source mineralogies [e.g., *Tepper et al.*, 1993; *Rushmer*, 1993; *Rapp and Watson*, 1995]. The main effect of increasing f_{H2O} is to prevent crystallization and removal of feldspar (plagioclase) from the melt by lowering the albite-anorthite solidus and destabilizing plagioclase as a residual mineral, thus generating melts with high Sr contents and minor negative Eu anomalies. Increasing Sr, Al_2O_3, and Na_2O contents indicate a decreasing role of plagioclase in the source mineralogy [*Beard and Lofgren*, 1991; *van der Laan and Wyllie*, 1992; *Sen and Dunn*, 1994]. Differentiation from mantle-derived basalt to dacite and rhyolite generally produces low Sr/Y ratios and extreme negative Eu anomalies owing to major feldspar (plagioclase) removal (see discussion by *Petford and Atherton* [1996]). The REE data of Late Cretaceous dacites-rhyolites and granodiorites-granites are characteristic for melting with f_{H2O} < 1 kbar, leaving a plagioclase + clinopyroxene residuum, whereas that of the late Eocene syntectonic/posttectonic granitoids (slightly negative or no Eu anomalies) requires amphibole in the source and is typical for higher f_{H2O} (f_{H2O} = 2–3 kbar [*Tepper et al.*, 1993]). The evolution of REE patterns of Late Cretaceous–Eocene arc magmatic rocks may therefore indicate gradually increasing meltwater fugacities with time.

Table 4. Geochemical Analyses of Representative Late Cretaceous–Eocene Samples From This Study, 52–48 Ma Arc[a]

	NN-D2	SS-C1c	L-A4/2	NN-C3	L-A1
Longitude, °W	68.738	69.415	69.034	68.681	69.02
Latitude, °S	21.697	24.717	22.51	21.713	22.514
Age, Ma	49.5 ± 1.6	49.7 ± 1.3			
Type	dike	lava	dike	intrusion	dike
SiO_2	48.15	51.03	55.82	56.13	56.58
TiO_2	0.98	1.10	1.10	0.72	1.18
Al_2O_3	18.09	16.54	17.32	17.70	17.99
FeO*	9.70	8.55	7.42	7.58	7.22
MnO	0.24	0.30	0.12	0.18	0.07
MgO	5.31	5.57	4.53	3.29	3.45
CaO	10.54	10.31	7.51	6.36	6.92
Na_2O	3.17	3.16	3.38	3.77	3.52
K_2O	2.40	1.99	1.75	3.22	2.03
P_2O_5	0.36	0.48	0.22	0.21	0.24
Total	98.92	99.05	99.17	99.16	99.20
LOI	3.52	1.33	0.35	1.42	1.23
La	16.5	14.7	21	28.0	25.1
Ce	34.2	34.1	61	55	54.0
Nd	19.5	19.4	23	25	25.7
Sm	4.17	4.18	ND	4.99	5.85
Eu	1.22	1.16	ND	1.22	1.52
Tb	0.616	0.681	ND	0.5	0.763
Y	15	17	18	21	20
Yb	1.77	2.02	ND	2.5	2.13
Lu	0.262	0.307	ND	0.4	0.315
Rb	33	40	47	104	62
Sr	801	548	484	924	479
Ba	1107	779	514	1556	510
Pb	12	5	8	14	11
Cs	7.06	1.54	ND	5.7	11.26
U	1.02	0.62	ND	4.4	1.19
Th	3.06	1.79	4	16.6	5.87
Zr	38	95	129	127	132
Hf	1.52	3.20	6	5.2	4.35
Nb	4	8	9	9	9
Ta	0.19	0.47	ND	0.5	0.66
Sc	30.7	32.9	19	18.05	24.1
Cr	41.0	179.9	48	8.7	51.4
Ni	14.0	32.0	18	5	34
Co	31.6	32.4	25	20.7	25.9
V	259	267	180	146	180
$^{87}Sr/^{86}Sr$	0.705172				
$^{87}Sr/^{86}Sr$ i	0.705081				
$^{143}Nd/^{144}Nd$	0.512680				
$^{143}Nd/^{144}Nd$ i	0.512700				
eNd	1.2				
$^{206}Pb/^{204}Pb$	18.588				
$^{206}Pb/^{204}Pb$ i	18.553				
$^{207}Pb/^{204}Pb$	15.649				
$^{207}Pb/^{204}Pb$ i	15.647				
$^{208}Pb/^{204}Pb$	38.658				
$^{208}Pb/^{204}Pb$ i	38.625				

[a] ND indicates not determined.

4.2. Sr-Nd-Pb Isotopes

[22] Late Cretaceous–Eocene arc magmatic rocks show relatively enriched initial Sr and Nd isotopic signatures compared to melts from the depleted asthenospheric mantle (Figure 3).

Table 5. Geochemical Analyses of Representative Late Cretaceous–Eocene Samples From This Study, 48-39 Ma Arc

	S-A1	N-E5	BB-33	SS-J6	SS-J7	N-F5	SS-D4	N-G1	SS-B1	S-A4	SS-L1	SS-C9	N-F3a	SS-J1	SS-C3	S-A5	NN-AF3	N-F3b	SS-H4	XR94-3[a]
Longitude, °W	69.075	68.994	69.008	69.066	69.081	68.899	69.77	68.887	69.804	69.143	68.999	69.694	68.896	69.369	69.486	69.132	68.87	68.894	69.388	68.6
Latitude, °S	23.007	21.771	22.65	23.152	23.152	21.794	24.921	21.815	25.295	23.15	22.546	24.854	21.808	23.675	24.711	23.194	21.861	21.807	24.089	23.5
Age, Ma	40.0 ± 1.3	40.2 ± 1.6	41.1 ± 1.1	43.8 ± 1.4																
Type	lava	tuff	lava	lava	intrusion	lava	lava	lava	lava	lava	lava	lava	tuff	lava	lava	lava	tuff	tuff	lava	lava
SiO_2	51.87	55.32	58.19	57.75	58.09	58.42	60.08	60.26	60.49	62.39	62.46	62.71	63.81	64.28	65.60	67.52	75.08	76.51	76.88	53.39
TiO_2	1.40	1.11	1.06	0.72	1.07	0.83	0.86	0.73	0.86	0.77	0.67	0.78	0.67	0.57	0.61	0.43	0.28	0.14	0.16	1.52
Al_2O_3	17.98	18.42	14.80	18.25	17.16	16.45	16.41	17.77	17.54	17.02	17.14	17.03	17.34	17.30	15.86	16.53	13.49	13.89	12.55	17.29
FeO*	9.78	7.02	4.60	6.18	5.79	6.76	5.55	5.30	5.60	5.09	4.49	5.40	4.68	4.41	4.15	2.92	1.74	0.77	0.87	7.98
MnO	0.17	0.07	0.09	0.13	0.08	0.16	0.10	0.13	0.07	0.20	0.08	0.10	0.09	0.09	0.06	0.05	0.02	0.01	0.04	0.14
MgO	3.28	2.47	3.77	3.33	3.97	2.51	3.65	1.73	2.30	3.54	2.51	1.68	1.54	1.50	1.83	1.34	1.03	0.97	0.23	4.82
CaO	9.11	8.70	8.68	6.26	5.77	9.01	6.46	6.74	5.65	3.82	4.86	5.03	5.52	4.24	4.09	2.79	2.70	3.46	0.84	6.30
Na_2O	3.33	4.19	5.42	4.46	3.77	3.34	3.51	4.54	4.14	3.54	4.12	3.52	3.08	4.64	3.39	4.67	1.53	2.57	3.37	4.62
K_2O	1.66	1.55	2.40	1.88	3.24	1.55	2.54	1.92	2.52	2.87	2.97	2.99	2.53	2.29	3.81	3.29	3.86	1.55	4.92	2.58
P_2O_5	0.32	0.36	0.48	0.35	0.42	0.20	0.24	0.27	0.20	0.19	0.20	0.16	0.22	0.20	0.12	0.13	0.07	0.04	0.03	0.47
Total	98.91	99.22	99.48	99.31	99.36	99.25	99.38	99.41	99.38	99.43	99.50	99.40	99.48	99.51	99.54	99.68	99.81	99.91	99.90	99.10
LOI	2.40	1.04	3.07	1.72	4.33	4.01	1.05	2.55	0.66	3.73	1.37	1.14	2.15	0.78	1.18	3.25	6.22	8.62	0.39	1.88
La	25.4	25.1	64.3	23.8	40.8	16.6	30.8	31.8	25.4	26.9	35.5	22.8	24.6	26.5	24.1	15.6	37.7	13.8	33.8	27.7
Ce	51	51	123	51.9	88.3	34	62.6	67.1	54.3	51	73.7	49.9	50	60.9	49.3	34	71.5	25	66.5	56
Nd	26	27	50	25.8	38.2	16	29.4	32.0	23.5	22	27.5	23.1	25	23.3	19.7	15	24.2	10	19.6	29
Sm	5.78	5.83	8.74	4.99	7.27	3.53	5.72	5.69	5.16	4.39	5.20	4.65	4.92	4.75	4.09	3.25	4.23	2.15	3.58	6.36
Eu	1.99	1.71	2.37	1.38	1.83	1.17	1.29	1.30	1.17	1.19	1.22	0.97	1.41	1.22	0.76	1.01	0.54	0.30	0.42	2.06
Tb	0.8	0.7	0.5	0.599	0.731	0.4	0.458	0.543	0.458	0.5	0.425	0.464	0.5	0.476	0.408	0.4	0.405	0.3	0.330	0.8
Y	17	14	13	17	20	12	20	15	20	17	21	18	20	18	22	15	21	17	30	24
Yb	2.4	1.6	1.1	1.95	1.54	1.3	1.49	1.65	1.50	1.3	1.46	1.49	2.1	1.60	1.49	1.0	1.49	1.3	1.43	2.8
Lu	0.4	0.2	0.1	0.304	0.229	0.2	0.216	0.243	0.216	0.2	0.211	0.226	0.3	0.242	0.231	0.1	0.230	0.2	0.221	0.4
Rb	31	41	39	37	65	22	71	46	82	95	100	75	82	59	116	84	94	46	203	75
Sr	935	915	1646	1048	726	527	923	761	573	454	620	771	601	499	330	950	1125	1301	125	562
Ba	592	349	729	567	1182	366	727	692	587	583	909	709	523	773	555	1056	803	655	573	524
Pb	6	5	15	8	13	5	12	10	12	9	15	13	11	10	12	5	15	10	24	6
Cs	1.1	1.0	0.5	0.60	2.19	0.5	4.37	0.81	4.63	3.0	3.65	1.72	1.7	1.03	4.80	5.2	2.79	1.5	5.31	2.4
U	0.7	1.0	1.7	0.86	1.93	0.6	3.43	1.24	3.39	2.5	2.60	2.55	1.1	1.84	5.11	1.2	3.63	2.8	5.31	0.70
Th	3.4	2.6	8.7	3.51	8.28	2.9	13.18	4.81	12.51	7.6	11.21	13.15	4.0	6.14	20.46	3.6	20.17	11.5	25.15	2.5
Zr	94	126	225	127	218	90	150	137	157	121	186	137	149	152	128	119	150	66	128	176
Hf	2.9	4.1	5.8	4.57	6.46	2.7	5.04	4.08	5.02	3.7	5.38	4.32	4.4	4.37	4.26	4.3	4.37	2.6	3.58	4.3
Nb	9	8	11	9	12	6	9	11	8	8	11	8	8	12	10	6	19	20	19	18
Ta	0.5	nd	0.5	0.58	0.78	nd	0.72	0.63	0.69	0.5	0.79	0.62	0.6	0.88	0.84	nd	1.43	1.4	1.64	1.2
Sc	24.72	17.06	14.18	12.6	14.2	16.15	15.7	9.5	15.4	11.88	10.9	13.2	10.55	8.1	10.4	6.07	3.3	3.62	1.6	23.02
Cr	30.1	18.5	157.6	9.7	47.0	11.8	102.0	21.3	31.8	20.2	29.3	20.5	11.3	6.8	19.2	14.8	1.6	6.5	nd	140.3
Ni	8	12	112	4	30	2	64	6	24	9	6	16	1	7.2	7	1	3.0	nd	0.7	66
Co	26.0	20.6	20.7	17.0	19.9	17.2	21.3	12.6	19.5	13.8	13.6	18.2	9.6	10.2	11.1	6.3	3.5	2.5	0.8	28.1
V	225	207	118	103	137	147	141	77	144	124	93	107	82	80	117	69	31	24	24	160
$^{87}Sr/^{86}Sr$											0.705157						0.705427			
$^{87}Sr/^{86}Sr$ i											0.704855						0.705265			
$^{143}Nd/^{144}Nd$											0.512712						0.512639			
$^{143}Nd/^{144}Nd$ i											0.512733						0.512667			
eNd											1.86						0.56			
$^{206}Pb/^{204}Pb$											18.691						18.773			
$^{206}Pb/^{204}Pb$ i											18.590						18.571			
$^{207}Pb/^{204}Pb$											15.631						15.612			
$^{207}Pb/^{204}Pb$ i											15.626						15.603			
$^{208}Pb/^{204}Pb$											38.733						38.734			
$^{208}Pb/^{204}Pb$ i											38.593						38.375			

[a] Back arc is represented.

This may indicate involvement of an enriched component such as old lithospheric mantle [*Rogers and Hawkesworth*, 1989] or continental crust [e.g., *Hildreth and Moorbath*, 1988; *Wörner et al.*, 1988; *Davidson et al.*, 1990; *Feeley and Davidson*, 1994]. Although Sr and Nd isotopic data of arc magmatic rocks show some isotopic enrichment with decreasing age, overall there is little contrast between Late Cretaceous ($^{87}Sr/^{86}S$ = 0.7039–0.7045 and $^{87}Nd/^{86}Nd$ = 0.51265–0.51276) and late Eocene rocks (mostly $^{87}Sr/^{86}S$ 0.7042–0.7046 and $^{87}Nd/^{86}Nd$ = 0.51263–0.51271). A major change is first seen between pre- and post-Miocene magmatic rocks [*Rogers and Hawkesworth*, 1989]. Only the initial Pb isotopic signature is characterized by systematically increasing initial $^{206}Pb/^{204}Pb$ ratios from 18.43–18.57 in Late Cretaceous volcanics to 18.53–18.70 in the late Eocene syntectonic/posttectonic granitoids. This range of initial Pb isotopic signatures lies intermediate between the fields of the northern and southern CVZ. However, Pb isotopic signatures are not only diagnostic of crustal thickening but may also reflect age, type, and structure of the crust [*Wörner et al.*, 1992; *Aitcheson et al.*, 1995]. The small contrast between Late Cretaceous and late Eocene main arc melts in terms of initial Sr and Nd isotopic ratios rules out major compositional, structural, or age changes during petrogenesis. Moreover, the less-enriched back arc alkaline rocks ($^{87}Sr/^{86}S$ = 0.7036–0.7046 and $^{87}Nd/^{86}Nd$ = 0.51280–0.51286) argue against isotopic enrichment by recycling of old mantle lithosphere during east propagating Andean arc magmatism, as proposed by *Rogers and Hawkesworth* [1989]. In addition, Late Cretaceous–Eocene magmatic rocks lack correlation between increasing initial Sr and Nd isotopic enrichment and increasing SiO_2 and decreasing Sr content (Figures 4a and 4b) in contrast to most younger central Andean silicic volcanic rocks which erupted through thicker crust [e.g., *Rogers and Hawkesworth*, 1989; *Wörner et al.*, 1988, 1994; *Trumbull et al.*, 1999]. This correlation is generally attributed to upper crustal contamination during low-pressure differentiation. Therefore the moderate Sr, Nd, and Pb isotopic enrichment in Late Cretaceous–Eocene main arc magmatic rocks may be due to higher pressure (deep crustal) enrichment.

5. Correlation of Late Cretaceous–Eocene Magma Source Variations With Crustal Thickening

[23] Partial melts of a deep (≥12 kbar) basaltic source will have the high La/Yb and Sr/Y ratios, low Yb and Y concentrations, and high Sr concentrations as seen in late Eocene syntectonic/posttectonic granitoids if both garnet and amphibole but minor or no plagioclase are residual in the source [e.g., *Rapp and Watson*, 1995; *Petford and Atherton*, 1996]. The presence of some residual amphibole is indicated by the concave upward REE pattern, low to moderate Rb/Sr and K/Rb ratios, and absent Eu anomalies. Even when amphibole is present, the onset of garnet stabilization at higher pressure deeper in the crust dramatically changes melt composition with an increase in SiO_2 content and decreases in FeO, MgO, Y, and Yb (as observed in the late Eocene magmatic rocks). The composition of melts from such sources resembles high-Al, low-K dacites (granodiorites) at 12 and 15 kbar, trondhjemites at 18 kbar [*Rushmer*, 1993], and also granodiorites and granites produced by dehydration melting of tonalite [*Singh and Johannes*, 1996]. The latter showed that changing pressure has little effect on the amount of melt fraction but controls the income and stabilization of (almandine rich) garnet (at 12 kbar at 900°C). Garnet may also be stabilized at lower pressures (8 kbar at 850°C) if the source is biotite-bearing [*Singh and Johannes*, 1996]. However, our model assumes that the main hydrous phase in newly underplated basaltic crust at ~12 kbar is amphibole, so that a biotite-bearing source seems unlikely in this case.

Table 6. Geochemical Analyses of Representative Late Cretaceous–Eocene Samples From This Study, 39–37 Ma Syntectonic/Posttectonic Arc

	NN-AD1a	NN-AD1a	NN-Q2 (1)	NN-Q2 (2a)	NN-Q2 (2b)
Longitude, °W	68.831	68.831	68.970	68.970	68.970
Latitude, °S	21.894	21.894	22.340	22.340	22.340
Type	intrusion	intrusion	intrusion	intrusion	intrusion
SiO_2	64.09	–	63.20	–	–
TiO_2	0.57	–	0.65	–	–
Al_2O_3	16.87	–	16.73	–	–
FeO*	4.27	–	4.76	–	–
MnO	0.07	–	0.08	–	–
MgO	1.91	–	2.24	–	–
CaO	4.34	–	4.58	–	–
Na_2O	4.21	–	4.13	–	–
K_2O	3.03	–	2.91	–	–
P_2O_5	0.16	–	0.20	–	–
Total	99.52	–	99.47	–	–
LOI	0.43	–	0.26	–	–
La	26.5	27.5	27.1	28.7	28.8
Ce	53.0	52	58.2	56	56
Nd	23.0	23	25.4	25	25
Sm	4.85	4.45	5.32	4.95	4.95
Eu	0.84	1.17	0.92	1.05	1.18
Tb	0.378	0.600	0.511	0.600	0.600
Y	22	22	22	22	22
Yb	1.41	1.3	1.54	1.4	1.4
Lu	0.171	0.2	0.221	0.2	0.3
Rb	108	120	94	114	112
Sr	612	612	612	612	612
Ba	661	668	664	686	693
Pb	13	13	12	12	12
Cs	4.65	4.9	5.36	5.8	6.0
U	5.05	4.6	3.92	3.4	3.5
Th	15.07	15.0	14.00	13.5	14.3
Zr	117	117	150	150	150
Hf	4.40	5.2	5.04	5.4	5.3
Nb	9	9	11	11	11
Ta	0.71	0.7	0.76	0.5	0.7
Sc	8.8	9.54	9.8	10.50	10.91
Cr	1.0	6.8	3.4	8.6	9.1
Ni	3	3	5	5	5
Co	11.4	12.0	13.1	13.5	14.3
V	70	70	102	102	102
$^{87}Sr/^{86}Sr$	0.704875		0.704863		
$^{87}Sr/^{86}Sr$ i	0.704508		0.704613		
$^{143}Nd/^{144}Nd$	0.512668		0.512694		
$^{143}Nd/^{144}Nd$ i	0.512630		0.512662		
eNd	0.96		1.42		
$^{206}Pb/^{204}Pb$	18.964		18.704		
$^{206}Pb/^{204}Pb$ i	18.701		18.529		
$^{207}Pb/^{204}Pb$	15.617		15.626		
$^{207}Pb/^{204}Pb$ i	15.605		15.618		
$^{208}Pb/^{204}Pb$	38.619		38.705		
$^{208}Pb/^{204}Pb$ i	38.368		38.504		

[24] Any explanation for the progressive increase in La/Yb and Sr/Y ratios through time (prior to Incaic crustal shortening) needs to take into account both increasing crustal thickening and mixing between underplated mantle-derived basalts and the generation of crustal melts from this newly underplated basaltic crust. We envisage a model in which progressive underplating of hot basalts at or near the base of the crust, due to establishment of a density barrier [*Laube and Springer*, 1998], triggers two parallel processes: (1) progressive deepening of the MASH zone through time, transforming initial lower-pressure gabbroic mineral assemblages to higher-pressure, garnet and amphibole-bearing source mineralogies, and (2) remelting of this newly underplated lower crust when

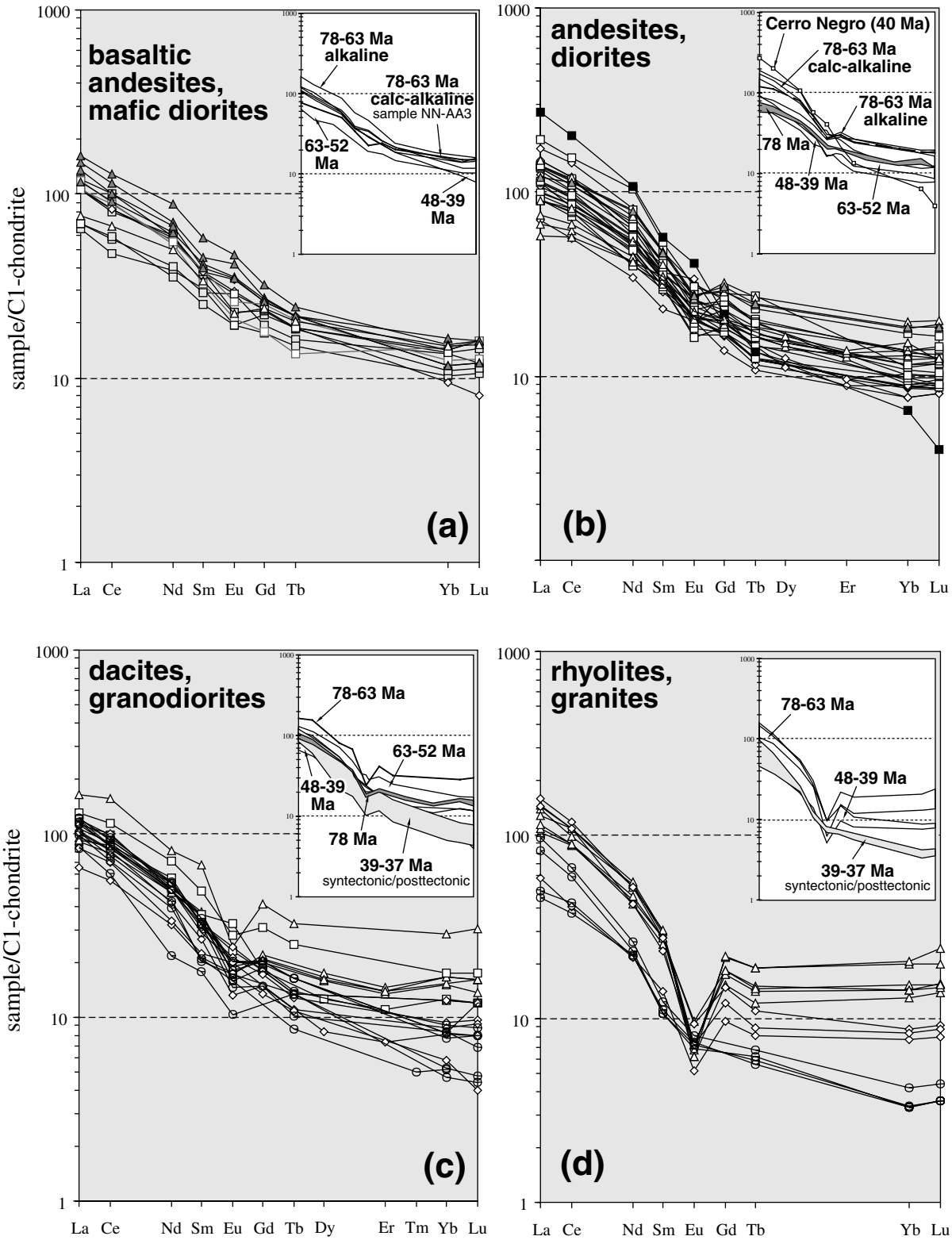

Figure 2. Rare earth element (REE) patterns of Late Cretaceous to late Eocene magmatic rocks in northern Chile. (a) Basaltic andesites and mafic diorites, (b) andesites and dorites, (c) dacites and granodiorites, and (d) rhyolites and granites. Insets show transition from largely overlapping mafic to intermediate REE patterns through time to increasing steepening of heavy REE patterns with increasing SiO_2 and decreasing age. More alkaline back arc magmatic rocks are characterized by light REE enrichment, relative to calc-alkaline arc rocks.

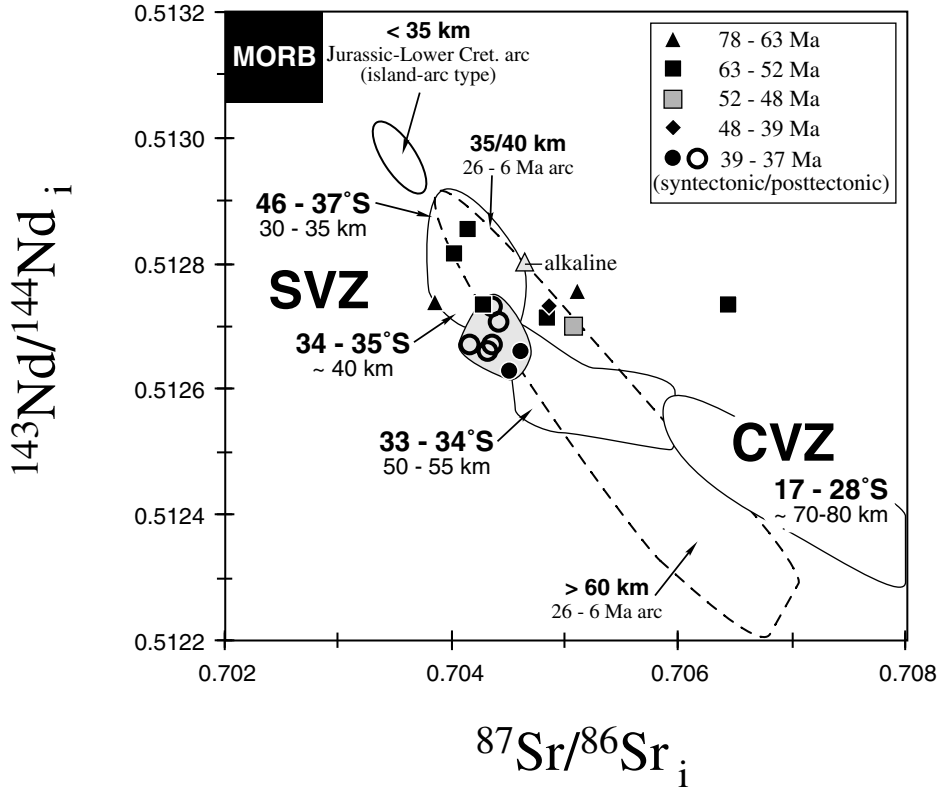

Figure 3. Initial $^{87}Sr/^{86}Sr$ isotopic ratios versus initial $^{143}Nd/^{144}Nd$ isotopic ratios of selected Late Cretaceous to late Eocene magmatic rocks versus rocks from other Andean arcs with variable crustal thickness. Late Cretaceous–Eocene rocks largely overlap with initial Sr and Nd isotopic composition in the southern volcanic zone (SVZ) between 37°S and 35°–34°S where crustal thicknesses are inferred to increase from 30–35 km to 40 km and in portions of the SVZ between 34° and 33°S where crustal thicknesses are thought to increase to 50–55 km. Initial Sr and Nd isotopic compositions of island arc-type Jurassic arc with thinner crust are generally less enriched, whereas SVZ rocks north of 34°S and late Miocene arc and central volcanic zone rocks with crust >50–55 km show more enriched signatures.

subsequently underplated hot mafic magmas release heat and water into the crustal environment, with crustal melt proportions increasing with time. By increasing crustal melt proportions we mean the gradually increasing percentage of crustal melt in the resulting hybrid between hot mantle-derived basalts and primary silicic melts from remelting (recycling) of newly underplated basaltic crust.

[25] Diagnostic thereof are the increasing La/Yb and Sr/Y ratios and the overall little Sr and Nd isotopic variation in the hybrid melt, since the (lower) crustal source consists of freshly underplated mantle basalts with little variation in composition and age. The predicted increase in more silicic rocks is consistent with diminishing and complete lack of mafic compositions in the late Eocene El Abra-Fortuna batholith.

[26] We simulated melting of different basaltic lower crustal garnet and/or amphibole-bearing source mineralogies at variable degrees of partial melting on Sr/Y versus Y and La/Yb versus Yb diagrams to test if partial melting of garnet-bearing basaltic lower crust can also explain the chemical signatures seen in the late Eocene granitoids (Figures 5a and 5b). Consistent with source compositions from previous batch melting models on basaltic crust [*Petford and Atherton*, 1996; *Drummond and Defant*, 1990], we used a basaltic source composition that was extracted from a slightly enriched upper mantle (enriched mid-ocean ridge basalt (EMORB), [after *Sun and McDonough*, 1989]). Source mineralogies vary from a hypothetical garnet-free amphibolite (amphibolite/garnet, 100/0) to garnet-bearing amphibolite (amphibolite/garnet, 90/10) to eclogite (amphibolite/clinopyroxene/garnet, 40/30/30) in order to account for increasing crustal thicknesses.

[27] Both the La/Yb and Sr/Y plots suggest that late Eocene syntectonic/posttectonic granitoids may be formed by partial melting of garnet-bearing amphibolite with up to 10 wt % garnet, whereas Late Cretaceous andesites-dacites-rhyolites (e.g., San Cristobal batholith at 78–76 Ma [*Maksaev*, 1990; *Pichowiak*, 1994; *Andriessen and Reutter*, 1994]) plot in the island-arc field and can be formed by differentiation from mantle-derived basalt (Figures 5a and 5b). Even melting of a hypothetical garnet-free amphibolite (amphibolite/garnet, 100/0) will not generate the high La/Yb and Sr/Y ratios seen in late Eocene syntectonic/posttectonic granitoids. Thus garnet was a residual mineral after Incaic tectonic crustal thickening, reflecting pressures $\geq$12 kbar or $\geq$40 km crustal thickness. Eclogitic residues (>10 wt % garnet) at pressures $\geq$15 kbar or $\geq$50 km crustal thickness produce overall higher La/Yb and Sr/Y ratios [*Rapp and Watson*, 1995] than those seen in the late Eocene granitoids, suggesting that crustal thicknesses at that time were <50 km. Garnet may form in basaltic bulk compositions by breakdown of amphibole + plagioclase under fluid-absent conditions by the following reaction: amphibole + plagioclase ± quartz = garnet + clinopyroxene + melt + new plagioclase at 12 and 18 kbar. Amphibole undergoes continuous reactions (at

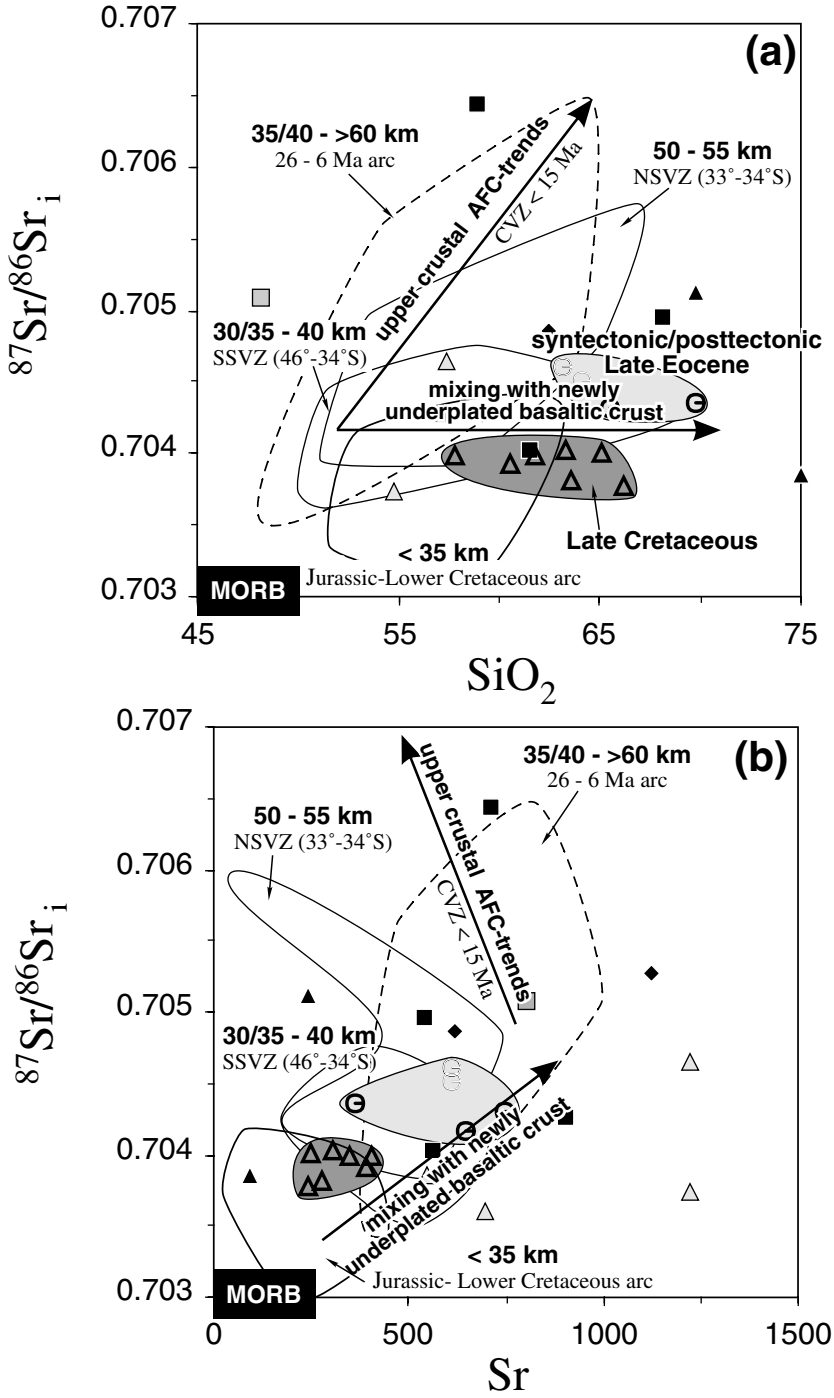

Figure 4. Initial $^{87}Sr/^{86}Sr$ isotopic ratios versus (a) SiO_2 (wt %) and versus (b) Sr concentrations (ppm) of selected rock suites from different arcs with variable crustal thicknesses show progressively increasing crustal contamination by upper crustal (lower pressure) assimilation/fractional crystallization (AFC) trends with increasing crustal thicknesses. Initial Sr isotopic enrichment of Late Cretaceous–Eocene magmatic rocks cannot be explained by upper crustal AFC processes but is consistent with signatures from melting and mixing with partial melts from newly underplated mafic crust.

935°–950°C) and remains stable with garnet up to at least 15 kbar. Successive breakdown of amphibole is responsible for gradually raising meltwater fugacities f_{H2O} (see section 4.1). At higher pressures (up to ~22 kbar), plagioclase and amphibole are destabilized as garnet and clinopyroxene are stabilized to (dry) eclogitic assemblages [*Rushmer*, 1993].

[28] Distribution coefficients used in our model are taken from *Martin* [1987]. Although the choice of distribution coefficients is difficult and somewhat arbitrary, our model is diagnostic of the mineral assemblages involved, and the distribution coefficients (KD) used for Yb in hornblende (hbl) (KD hbl_{Yb} = 1.7 [*Martin*, 1987]) are within the range of those

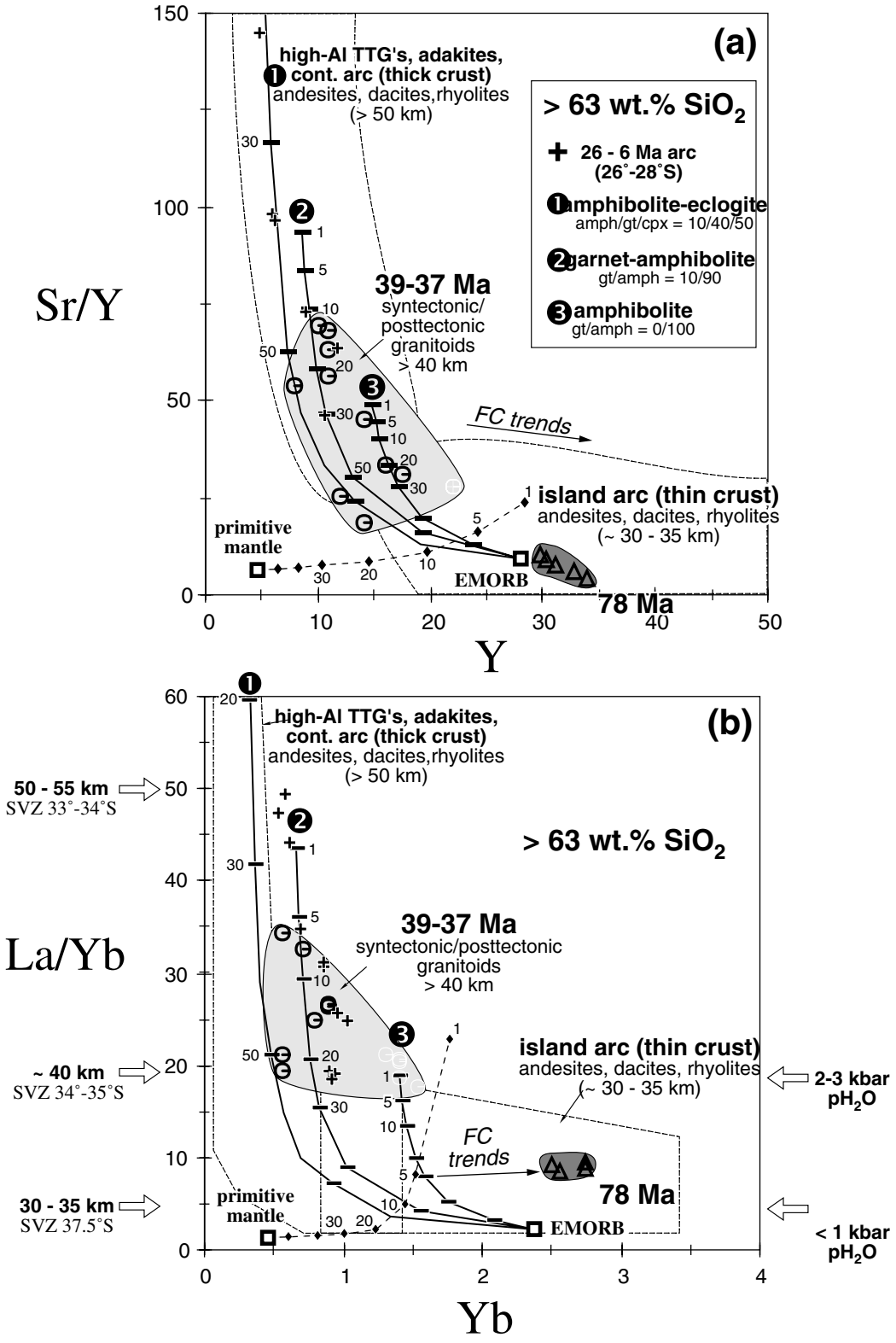

Figure 5. Plot of (a) Sr/Y versus Y and (b) La/Yb versus Yb of silicic (>63 wt % SiO_2) Late Cretaceous and late Eocene magmatic rocks. Area of narrow hatching shows samples from the 78 Ma old intrusive plotting in island-arc andesite-dacite-rhyolite field with thin crust. Area of wide hatching shows samples from 39 to 37 Ma old syntectonic/posttectonic El Abra-Fortuna batholith that overlaps field of arcs with thick crust and high-Al trondhjemite-tonalite-granodiorite (TTG) and adakite fields [after *Drummond and Defant*, 1990]. Enriched mid-ocean ridge basalt (EMORB) source after *Sun and McDonough* [1989] and *Drummond and Defant* [1990]. Correlating crustal thicknesses are from *Hildreth and Moorbath* [1988], and H_2O fugacities are from *Tepper et al.* [1993].

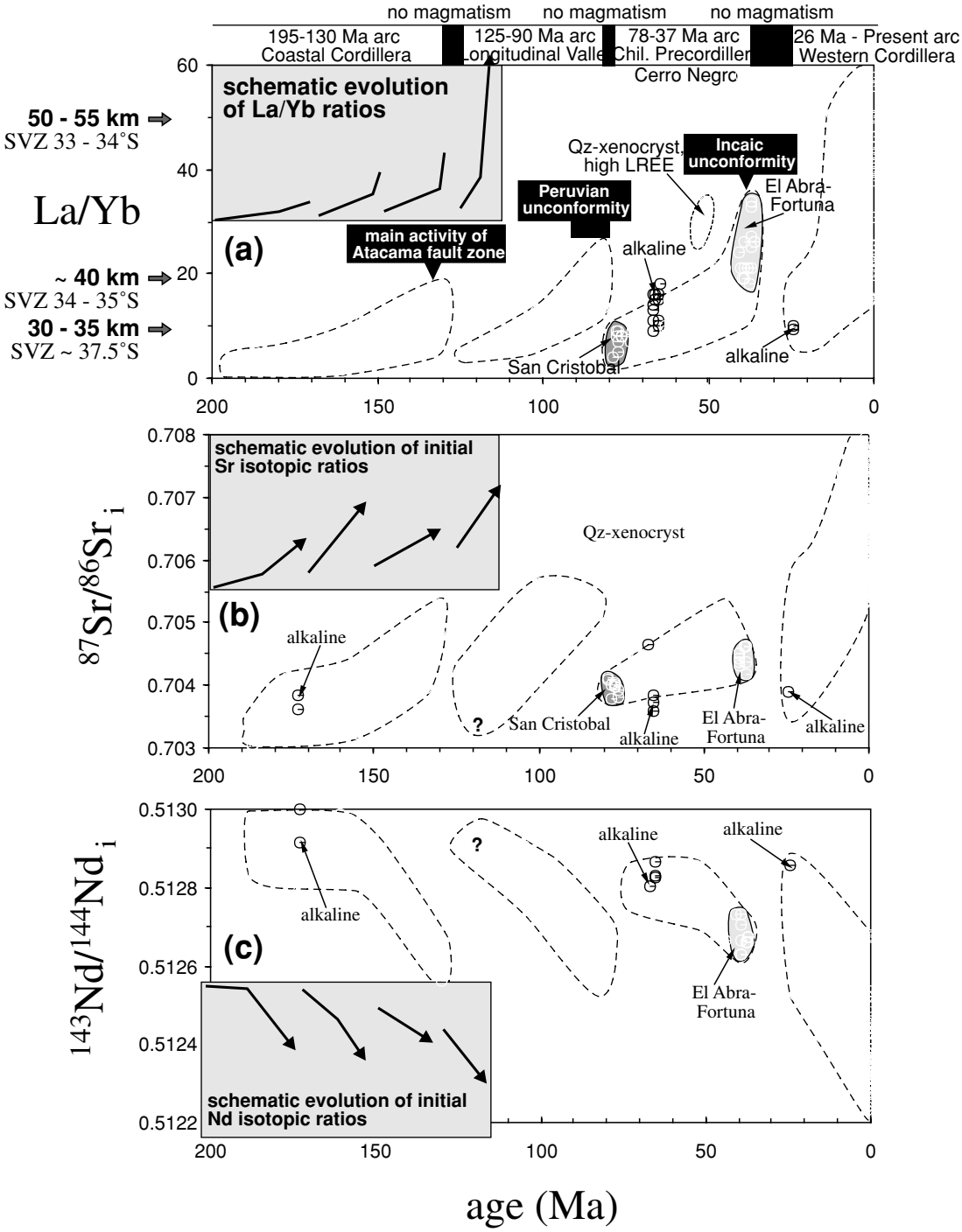

Figure 6. Plot of age of Andean magmatic rocks (a) versus La/Yb, (b) versus initial $^{87}Sr/^{86}Sr$ ratios, and (c) versus $^{143}Nd/^{143}Nd$ isotopic ratios showing correlation of steepening REE patterns and increasing isotopic enrichment with decreasing age within each individual arc system and with increasing arc crustal thickening. Periods without arc magmatism follow tectonic activity along the arc by transpressional-transtensional fault movements or across the arc by horizontal shortening of the crust and correlate with stepwise migration of arc magmatic activity to the east.

determined in recent studies (KD hbl_{Yb} = 1.15–2.10 [see *Klein et al.*, 1997]). Recent studies on trace element partitioning in garnet [e.g., *van Westrenen et al.*, 1999] also revealed a range of partition coefficients for Yb in garnet depending on the crystal composition. Using a range of partition coefficients will produce a range of modeled La/Yb and Sr/Y ratios, but it will not change the general effect of increasing La/Yb and Sr/Y ratios with increasing hornblende and/or garnet. The purpose of our simple modeling is to determine major mineralogical changes after the Incaic crustal thickening and to indicate its effect on melt production, not to imply that processes as simple as these actually occurred.

[29] The geochemical and initial Sr and Nd isotopic characteristics prior to Incaic deformation are also similar to those

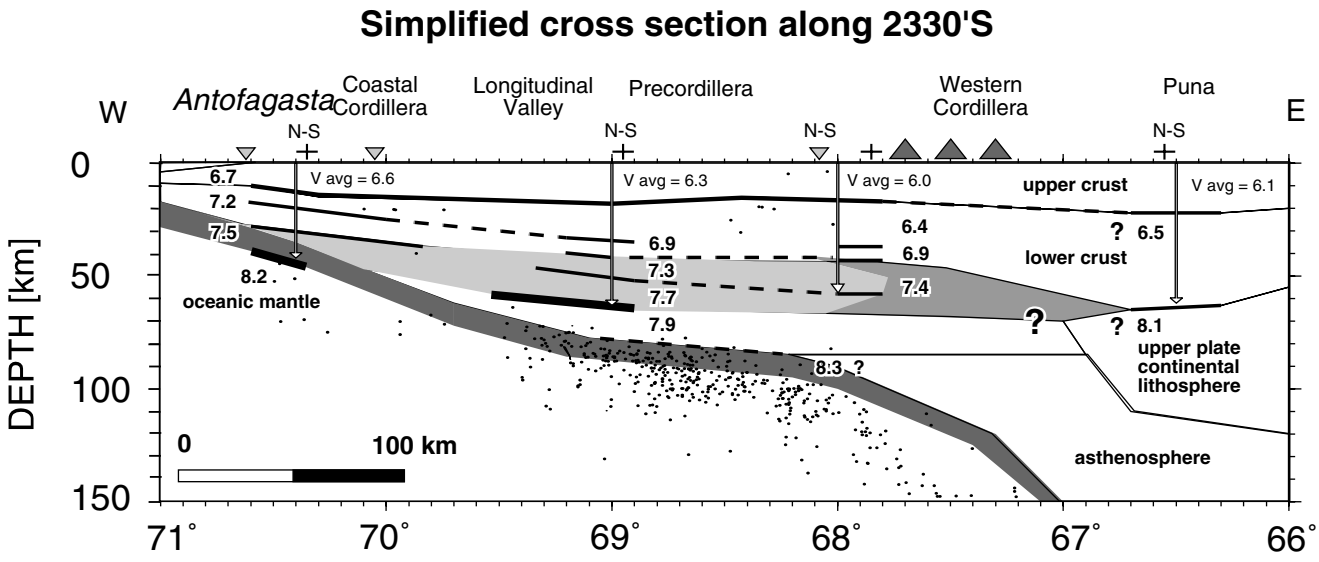

Figure 7. Simplified seismic section across the central Andes at 23°30′S [after *Lessel*, 1998]. Note lower crustal seismic *P* wave velocities of 7.3–7.7 km (light shading) lying within the range of newly underplated mafic amphibole and garnet-bearing crust predicted by *Furlong and Fountain* [1986]. Solid dots reflect seismic activity in the subducting oceanic slab (dark shading), solid curves indicate strong crustal reflectors, and arrows point to location of N–S seismic profiles.

from the southern SVZ between 37° and 34°S (Figures 3, 4a, and 4b), where inferred crustal thicknesses increase from 30–35 to ~40 km [*Hildreth and Moorbath*, 1988]. The REE signatures and initial Sr and Nd isotopic ratios of late Eocene syntectonic/posttectonic granitoids overlap the field of late Oligocene volcanic rocks in the Maricunga belt (26°–28°S [*Kay et al.*, 1994]) and that of the southern SVZ between 35° and 34°S, where crustal thicknesses of ~40 km were estimated [*Hildreth and Moorbath*, 1988]. On the basis of isostasy and comparison with other regions, SVZ volcanic rocks between 34° and 33°S are thought to have passed through 50 to 55-km-thick crust. Most initial Sr and Nd isotopic compositions of late Eocene syntectonic/posttectonic rocks are less enriched than SVZ volcanic rocks, and only the late Eocene syntectonic/posttectonic granitoids partly overlap this SVZ field (Figures 3, 4a, and 4b). Using these along arc geochemical and crustal thickness variations as an analog, we assume that Late Cretaceous to middle late Eocene magmatic underplating may have thickened the crust by ~5–10 km, from 30–35 km to ~40 km. Subsequent late Eocene Incaic shortening and thickening of the crust lowered the arc crustal base, and therefore the MASH zone, to ~45 km, an assumption consistent with the overall amount of Incaic crustal thickening (14.5% [*Günther et al.*, 1998]).

6. Correlation of Pre-Neogene Geochemical Variations With Changing Tectonic Settings

[30] Geochemical changes revealed by the partially eroded pre-Neogene magmatic paleoarcs in north Chile provide important constraints on the relative timing of magmatic and tectonic events associated with changes in plate convergence parameters. This kind of access is not available in the Western Cordillera, where modern stratovolcanoes cover older and deeper structures.

[31] During the Late Cretaceous the lowest La/Yb and Sr/Y ratios and least enriched Sr and Nd isotopic ratios (e.g., San Cristobal intrusive complex) correlate with low plate convergence rates and highly oblique subduction, incipient back arc rifting, and alkaline back arc magmatic activity (Figures 6a–6c). Subsequently, increasing but moderate La/Yb and Sr/Y ratios in Paleocene to Eocene magmatic rocks were associated with decreasing obliquity of subduction and increasing convergence rates in a "transitional" tectonic regime. At the same time, crustal extension and alkaline magmatic activity terminated as the main arc magmatic activity gradually migrated eastward. Arc migration ended with formation of monogenetic centers along NW-SE trending fracture zones across the arc (Cerro Negro and Cerro Olivino). The very high La/Yb ratios (up to 58) of these mainly dark, glassy magmatic rocks are due to high La concentrations. The highest La/Yb and Sr/Y ratios are found in late Eocene syntectonic/posttectonic granitoids of the El Abra-Fortuna batholith (Figure 6a). Emplacement of these intrusions correlates with Incaic tectonic shortening (38.5 Ma [*Döbel et al.*, 1992]) and crustal thickening prior to the termination of arc magmatism at ~37 Ma.

[32] This sequential pattern of arc magmatism and crustal shortening is characteristic of all Andean magmatic episodes in north Chile (Peruvian at 90-80 Ma, Incaic at 38.5 Ma, and Quechua at ~10 Ma), except for the Jurassic arc (Figure 6a) where there is no evidence for crustal shortening or significant crustal thickening, consistent with overall constant La/Yb ratios with time and low Sr/Y ratios. In the mid-Cretaceous arc the Peruvian unconformity indicates some shortening and thickening of the crust between 90 and 80 Ma [*Scheuber et al.*, 1994], and although the temporal evolution pattern is not well constrained (owing to a lack of outcrops), the overall trend of increasing La/Yb ratios is clear. Using the known present geodynamic setting, we can make the following inferences about the geometry of pre-Neogene subduction. Like in modern regions with subhorizontal subduction (flat slab), termination and lack of arc magmatic activity after each tectonic episode can be attributed to flat subduction at high convergence rates. This pattern may, in fact, imply that repeated periods of flat slab subduction are a characteristic feature of the entire Andean orogeny, making pre-Andean magmatic periods analogous to the present flat slab subduction regions. This problem is addressed in more detail in a separate paper [*Haschke et al.*, 2001].

7. Implications of Mafic Underplating on Geophysical Properties of Andean Lower Crust

[33] Addition of substantial amounts of mafic magma to the base of the continental crust will have significant effects on the geophysical nature of the lower crust and crust-mantle boundary. After crystallization the velocity structure within the underplated layers will depend on the mineralogical composition, pressure, and temperature. Using our modeled residual mineralogy variations, residues of late Eocene syntectonic/posttectonic granitoids presumably consisted of amphibole + clinopyroxene ± plagioclase ± garnet (<10 wt %) (see discussion in section 5). Estimated densities of such solid residues range from ~2.95 g cm^{-3} for the garnet-free pre-Incaic source to ~3.13 g cm^{-3} for the garnet-bearing syntectonic/posttectonic source [*Furlong and Fountain*, 1986; *Rushmer*, 1993; *Petford and Atherton*, 1996]. Seismic velocities of such residues can be approximated from measured *P* and *S* wave velocities for individual minerals [*Toft et al.*, 1989]. The lower crustal *P* wave velocity (V_p) beneath the Coastal Cordillera, Longitudinal Valley, Chilean Precordillera and Western Cordillera at 23.5°S ranges between 7.3 and 7.7 km s^{-1} (Figure 7). This range of *P* wave velocities is well within the interval expected for magmatic underplating (7.1–7.8 km s^{-1} [*Furlong and Fountain*, 1986; *Rushmer*, 1993]). Furthermore, the minimum amount of crustal thickening needed to balance Late Cretaceous to Eocene crustal thickening (5–10 km [*Haschke*, 1999]) agrees with the thickness of the 7.3–7.7 km s^{-1} velocity layers and is well within the potential range of magmatic underplating (up to 25 km) as predicted by *Furlong and Fountain* [1986]. The presence of low-velocity zones beneath the magmatically active Western Cordillera (V_p ~6.0 km s^{-1} [*Schmitz*, 1994; *Schmitz et al.*, 1999]) is consistent with the earlier proposition that the lower crust in northern Chile is mafic, relatively dense, and hot and that magmatic underplating is an ongoing process.

8. Summary and Conclusions

[34] Increasing La/Yb and Sr/Y ratios and increasing Sr and Nd isotopic enrichment with time are characteristic not only of Neogene magmatic rocks but of pre-Neogene Andean magmatic episodes in north Chile as well (Figures 6a–6c). These temporal geochemical changes reflect a progressive transfer of melting zone from the upper mantle into variably thickened garnet-bearing (lower) crust.

[35] Arc crustal thicknesses in Andean magmatic arcs evolved from overall low (island-arc type) crustal thicknesses of ~30–35 km in the Jurassic arc to ~45 km in late Eocene after Incaic crustal shortening. Since most of the magmatic activity during this time occurred during extensional tectonic regimes and shortening of the crust was restricted to transpressive tectonic episodes, most of the crustal thickening must be due to other mechanisms. Hydration of mantle peridotite and/or underplating of tectonically eroded forearc material may explain the relatively low *P* wave velocities at a depth of 70 km beneath the central Andean forearc but cannot explain the systematically changing melt compositions and isotopic signatures through time seen in Andean magmatic rocks. Newly underplated basaltic crust can account for the missing crustal volume after shortening. The Neogene arc was established on thickened continental crust older than 26 Ma. Most important, magmatic recycling of this mafic underplate can explain the evolution of geochemical signatures in Andean arc magmatic rocks. The source for gradual thermal crustal weakening and magmatic recycling are the hot underplated basalts themselves.

[36] A similar recent evolutionary trend has been described in central Chile. *Parada et al.* [1999] recognized a magmatic evolution from enriched Sr and Nd isotope signatures during the Carboniferous to depleted signatures during the Early Jurassic–Cretaceous for the mafic rocks between 31° and 34°S.

[37] Underplating mantle-derived basaltic crust also helps in solving a notorious problem with magmatic addition and its contribution to crustal growth, as earlier estimates of average magmatic addition rates in subduction zones commonly used volumes of volcanic and plutonic rocks seen at the surface (see *Kono et al.* [1989] for a review); these rates are far too low to explain the crustal volume of the central Andes. Our model incorporates and supports elements of earlier models [e.g., *James*, 1971; *Suarez et al.*, 1983; *Kono et al.*, 1989; *Schmitz*, 1994] by suggesting differential partitioning of deformation, such that tectonic crustal thickening dominated in the Altiplano-Puna plateau and Eastern Cordillera, whereas magmatic underplating is needed to balance crustal thickening beneath the present magmatic arc.

[38] The present magmatic arc of the Western Cordillera in north Chile, NW Argentina, and SW Bolivia is subject to rapid and almost arc-normal convergence and mainly transpressional stresses. Similar to pre-Neogene episodes of the Andean orogeny, this might indicate onset of a period of crustal shortening and tectonic crustal thickening; before-present arc magmatism in the Western Cordillera will end with very high La/Yb and Sr/Y ratios and enriched Sr and Nd isotopic signatures, and future Andean arc magmatism will establish farther east, with low La/Yb and Sr/Y and less enriched Sr and Nd isotopic ratios.

[39] **Acknowledgments.** This work is a synthesis of a doctoral thesis by Michael Haschke (1999). We are indebted to the Universidad Catolica del Norte and Tomislav Bogdanic in Chile for field assistance and to the GFZ Potsdam for use of analytical facilities. Many fruitful discussions with K.-J. Reutter, Matt Gorring, and Rolf Kilian are gratefully acknowledged, as is Gerhard Wörners help drafting the manuscript. Constructive reviews of Hikaru Iwamori, Miguel Parada, and one anonymous reviewer substantially helped improve an earlier version of this manuscript. Our work has been supported by the Collaborative Research Program "Deformation Processes in the Andes" (SFB 267) at the Free University of Berlin, Germany.

References

Aitcheson, S. J., R. S. Harmon, S. Moorbath, A. Schneider, P. Soler, E. Soria-Escalante, G. Steele, I. Swainbank, and G. Wörner, Pb isotopes define basement domains of the Altiplano, central Andes, *Geology*, *23*, 555–558, 1995.

Allmendinger, R. W., T. E. Jordan, S. M. Kay, and B. L. Isacks, The evolution of the Altiplano-Puna plateau of the central Andes, *Annu. Rev. Earth Planet. Sci.*, *25*, 139–174, 1997.

Andriessen, P. A., and K.-J. Reutter, K-Ar and fission track mineral age determination of igneous rocks to multiple magmatic arc systems along the 23°S latitude of Chile and NW Argentina, in *Tectonics of the Southern Central Andes*, edited by K.-J. Reutter, E. Scheuber, and P. Wigger, pp. 141–153, Springer-Verlag, New York, 1994.

Atherton, M. P., and N. Petford, Generation of sodium-rich magmas from newly underplated basaltic crust, *Nature*, *362*, 144–146, 1993.

Beard, J. S., and G. E. Lofgren, Dehydration melting and water-saturated melting of basaltic and andesitic greenstones and amphibolites at 1, 3, and 6.9 kbar, *J. Petrol.*, *32*, 365–401, 1991.

Charrier, R., and K.-J. Reutter, The Purilactis Group of northern Chile: Boundary between Arc and Backarc from late Cretaceous to Eocene, in *Tectonics of the Southern Central Andes*, edited by K.-J. Reutter, E. Scheuber, and P. Wigger, pp. 189–202, Springer-Verlag, New York, 1994.

Coira, B., J. Davidson, C. Mpodozis, and V. A. Ramos, Tectonic and magmatic evolution of the Andes of northern Argentina and Chile, *Earth Sci. Rev.*, *18*, 303–332, 1982.

Davidson, J. P., N. McMillan, S. Moorbath, G. Wörner, R. Harmon, and L. Lopez-Escobar, The Nevados de Payachata volcanic region (18°S/69°W, N. Chile), 2, Evidence for widespread crustal involvement in Andean magmatism, *Contrib. Mineral. Petrol.*, *105*, 412–432, 1990.

Dilles, J. H., A. J. Tomlinson, M. W. Martin, and N. Blanco, El Abra and Fortuna complexes: A porphyry copper batholith sinistrally displaced by the Failla Oeste, VIII, *Congr. Geol. Chileno Actas*, *3*, 1883–1887, 1997.

Döbel, R., K. Hammerschmidt, and H. Friedrichsen, Implication of $^{40}Ar/^{39}Ar$ dating of early Tertiary volcanic rocks from the north-Chilean Precordillera, *Tectonophysics*, *202*, 55–81, 1992.

Drummond, M. S., and M. J. Defant, A model for trondhjemite-tonalite-

dacite genesis and crustal growth via slab melting: Archean to modern comparisons, *J. Geophys. Res.*, *95*, 21,503–21,521, 1990.

Feeley, T. C., and J. P. Davidson, Petrology of calc-alkaline lavas at Volcan Ollagüe and the origin of compositional diversity at central Andean stratovolcanoes, *J. Petrol.*, *35*, 1295–1340, 1994.

Francis, P. W., and C. J. Hawkesworth, Late Cenozoic rates of magmatic activity in the central Andes and their relationships to continental crust formation and thickening, *J. Geol. Soc. London*, *151*, 845–854, 1994.

Furlong, K., and D. M. Fountain, Continental crustal underplating: Thermal considerations and seismic-petrological consequences, *J. Geophys. Res.*, *91*, 8285–8294, 1986.

Günther, A., M. R. Haschke, K.-J. Reutter, and E. Scheuber, Kinematic evolution and structural geometry of the Chilean Precordillera (21.5–23°S): Inversional tectonics in the Late Cretaceous-Paleogene magmatic arc, *Terra Nostra Abstr.*, *98*(5), 58–59, 1998.

Haschke, M. R., Variationen in der Magmengenese oberkretazischer bis obereozäner Magmatite in Nordchile (21.5–26°S), *Berl. Geowiss. Abh.*, *201*, 130 pp., 1999.

Haschke, M. R., E. Scheuber, A. Günther, and K.-J. Reutter, Evolutionary cycles during the Andean orogeny: Repeated slab breakoff and flat subduction?, *Terra Nova*, in press, 2001.

Heumann, A., G. Anthes, and G. Wörner, Geochemical and isotopical variations of Upper Cretaceous and Tertiary intrusive rocks along the north Chilean precordillera (18°–22°S), *Eos Trans. AGU*, *74*(43), Fall Meet. Suppl., 638, 1993.

Hickey, R. L., F. A. Frey, D. C. Gerlach, and L. Lopez-Escobar, Multiple sources for basaltic rocks from the southern volcanic zone of the Andes (34°–41°S): Trace element and isotopic evidence for contributions from subducted oceanic crust, mantle, and continental crust, *J. Geophys. Res.*, *91*, 5963–5983, 1986.

Hildreth, W., and S. Moorbath, Crustal contributions to arc magmatism in the Andes of central Chile, *Contrib. Mineral. Petrol.*, *98*, 455–489, 1988.

Isacks, B. L., Uplift of the central Andean Plateau and bending of the Bolivian orocline, *J. Geophys. Res.*, *93*, 3211–3231, 1988.

James, D. E., Andean crustal and upper mantle structure, *J. Geophys. Res.*, *76*, 3246–3271, 1971.

Kay, S. M., V. Maksaev, C. Mpodozis, R. Moscoso, and C. Nasi, Probing the evolving Andean lithosphere: Mid-late Tertiary magmatism in Chile (29°–30.5°S) over the zone of subhorizontal subduction, *J. Geophys. Res.*, *92*, 6173–6189, 1987.

Kay, S. M., V. A. Ramos, C. Mpodozis, and P. Sruoga, Late Paleozoic to Jurassic silicic magmatism at the Gondwanaland margin: Analogy to the middle Proterozoic in North America?, *Geology*, *17*, 324–328, 1989.

Kay, S. M., C. Mpodozis, V. A. Ramos, and F. Munizaga, Magma source variations for mid-Tertiary magmatic rocks associated with a shallowing subduction zone and a thickening crust in the central Andes (28°–33°S), in *Andean Magmatism and Its Tectonic Setting*, edited by R. S. Harmon and C. W. Rapela, *Spec. Pap. Geol. Soc. Am.*, *265*, 113–137, 1991.

Kay, S. M., C. Mpodozis, A. Tittler, and P. Cornejo, Tertiary magmatic evolution of the Maricunga mineral belt in Chile, *Int. Geol. Rev.*, *36*, 1079–1112, 1994.

Klein, M., H. G. Stosch, and H. A. Seck, Partitioning of high field-strength and rare-earth elements between amphibole and quartz-dioritic to tonalitic melts: An experimental study, *Chem. Geol.*, *138*, 257–271, 1997.

Kono, M., Y. Fukao, and A. Yamamoto, Mountain building in the central Andes, *J. Geophys. Res.*, *94*, 3891–3905, 1989.

Kramer, W., G. Haase, R. Romer, and W. Siebel, Temporal magma chemical trends in the Jurassic volcanic arc near Iquique (20°30′S) and Arica (18°30′S), north Chilean coastal range, isotope- and element chemical constraints, *Terra Nostra Abstr.*, *98*(5), 93, 1998.

Laube, N., and J. Springer, Crustal melting by ponding of mafic magmas: A numerical model, *J. Volcanol. Geotherm. Res.*, *81*, 19–35, 1998.

Lessel, K., Die Krustenstruktur der Zentralen Anden in Nordchile (21–24°S), abgeleitet aus 3D-Modellierungen refraktionsseismischer Daten, *Berl. Geowiss. Abh.*, *B-31*, 185 pp., 1998.

Lucassen, F., and G. Franz, Arc related Jurassic igneous and meta-igneous rocks in the coastal cordillera of northern Chile region Antofagasta, *Lithos*, *32*, 273–298, 1994.

Maksaev, V., Metallogeny, geological evolution, and thermochronology of the Chilean Andes between latitudes 21° and 26°S and the origin of major porphyry copper deposits, Ph.D. thesis, 554 pp., Dalhousie Univ., Halifax, N. S., Canada, 1990.

Martin, H., Petrogenesis of Archean trondhjemites, tonalites and granodiorites from eastern Finland: Major and trace element geochemistry, *J. Petrol.*, *28*, 921–953, 1987.

McMillan, N. J., R. S. Harmon, S. Moorbath, L. Lopez-Escobar, and D. F. Strong, Crustal sources involved in continental arc magmatism: A case study of volcan Mocho-Choshuenco, southern Chile, *Geology*, *17*, 1152–1156, 1989.

McMillan, N., J. Davidson, G. Wörner, R. S. Harmon, L. Lopez-Escobar, and S. Moorbath, Mechanism of trace element enrichment related to crustal thickening: The Nevados de Payachata region, northern Chile, *Geology*, *21*, 467–470, 1993.

Mpodozis, C. M., N. S. Marinovic, I. T. Smoje, and L. G. Cuitino, Estudio Geologico—Estructural de la Cordillera de Domeyko entre Sierra Limon Verde y Sierra Mariposas Region de Antofagasta, map, 281 pp., scale 1:100,000, Serv. Nac. de Geol. y Minera Corp. Nac. del Cobre de Chile, Santiago, 1993.

Parada, M. A., J. O. Nyström, and B. Levi, Multiple sources for the coastal batholith of central Chile (31–34°S): Geochemical and Sr-Nd isotopic evidence and tectonic implications, *Lithos*, *46*, 505–521, 1999.

Pardo-Casas, F., and P. Molnar, Relative motion of the Nazca (Farallon) and South American plates since Late Cretaceous time, *Tectonics*, *6*, 233–248, 1987.

Peacock, S. M., T. Rushmer, and A. B. Thompson, Partial melting of subducting oceanic crust, *Earth Planet. Sci. Lett.*, *121*, 227–244, 1994.

Petford, N., and M. Atherton, Na-rich partial melts from newly underplated basaltic crust: The Cordillera Blanca batholith, Peru, *J. Petrol.*, *37*, 1491–1521, 1996.

Pichowiak, S., Early Jurassic to Early Cretaceous magmatism in the coastal cordillera and the central depression of north Chile, in *Tectonics of the Southern Central Andes*, edited by K.-J. Reutter, E. Scheuber, and P. Wigger, pp. 203–217, Springer-Verlag, New York, 1994.

Rapp, R. P., and E. B. Watson, Dehydration melting of metabasalt at 8–32 kbar: Implications for continental growth and crust-mantle recycling, *J. Petrol.*, *36*, 891–931, 1995.

Reymer, A., and G. Schubert, Phanerozoic addition rates to the continental crust and crustal growth, *Tectonics*, *3*, 63–77, 1984.

Roeder, D., Andean-age structure of eastern Cordillera, province of La Paz, Bolivia, *Tectonics*, *7*, 23–39, 1988.

Rogers, G., and C. J. Hawkesworth, A geochemical traverse across the north Chilean Andes: Evidence for crust generation from the mantle wedge, *Earth Planet. Sci. Lett.*, *91*, 271–285, 1989.

Rushmer, T., Experimental high pressure granulites: Some applications to natural mafic xenolith suites and Archean granulite terranes, *Geology*, *21*, 411–414, 1993.

Rutland, R. W., Andean orogeny and sea floor spreading, *Nature*, *233*, 252–255, 1971.

Scheuber, E., T. Bogdanic, A. Jensen, and K.-J. Reutter, Tectonic development of the north Chilean Andes in relation to plate convergence and magmatism since the Jurassic, in *Tectonics of the Southern Central Andes*, edited by K.-J. Reutter, E. Scheuber, and P. Wigger, pp. 121–139, Springer-Verlag, New York, 1994.

Schmitz, M., A balanced model of the southern central Andes, *Tectonics*, *13*, 484–492, 1994.

Schmitz, M., et al., The crustal structure beneath the central Andean forearc and magmatic arc as derived from seismic studies–The PISCO 94 experiment in northern Chile (21–23°S), *J. South Am. Earth Sci.*, *12*(3), 237–260, 1999.

Sen, C., and T. Dunn, Dehydration melting of basaltic composition amphibolite at 1.5 and 2.0 GPa: Implications for the origin of adakites, *Contrib. Mineral. Petrol.*, *117*, 394–409, 1994.

Sheffels, B. M., Lower bound on the amount of crustal shortening in the central Bolivian Andes, *Geology*, *18*, 812–815, 1990.

Singh, J., and W. Johannes, Dehydration melting of tonalities, Part II, Composition of melts and solids, *Contrib. Mineral. Petrol.*, *125*, 26–44, 1996.

Somoza, R., Updated Nazca (Farallon)-South America relative motions during the last 40 m.y.: Implications for mountain building in the central Andean region, *J. South Am. Earth Sci.*, *11*(3), 211–215, 1998.

Stern, C. R., K. Futa, and K. Muchlenbacks, Isotopic and trace element data for orogenic andesites from the Austral Andes, in *Andean Magmatism, Chemical and Isotopic Constraints*, edited by R. S. Harmon and B. A. Barreiro, pp. 31–46, Shiva, San Ramon, Calif., 1984.

Suarez, G., P. Molnar, and B. C. Burchfiel, Seismicity, fault plane solutions, depth of faulting, and active tectonics of the central Andes, *J. Geophys. Res.*, *88*, 403–428, 1983.

Sun, S.-S., and W. F. McDonough, Chemical and isotopic systematics of oceanic basalts: Implications for mantle composition and processes, in *Magmatism in the Ocean Basins*, edited by A. D. Saunders and M. J. Norry, *Geol. Soc. Am. Spec. Publ.*, *42*, 313–345, 1989.

Tepper, J. H., B. K. Nelson, G. W. Bergantz, and A. J. Irving, Petrology of the Chilliwack batholith, North Cascades, Washington: Generation of calc-alkaline granitoids by melting of mafic lower crust with variable water fugacity, *Contrib. Mineral. Petrol.*, *113*, 333–351, 1993.

Toft, P. B., D. V. Hills, and S. E. Haggerty, Crustal evolution and the granulite eclogite transition in xenoliths from kimberlites in the west African craton, *Tectonophysics*, *161*, 213–231, 1989.

Trumbull, R. B., R. Wittenbrink, K. Hahne, R. Emmermann, W. Büsch, H. Gerstenberger, and W. Siebel, Evidence for late Miocene to recent contamination of arc andesites by crustal melts in the Chilean Andes (25–

26°S) and its geodynamic implications, *J. South Am. Earth Sci.*, *12*(2), 135–155, 1999.

van der Laan, S. R., and P. J. Wyllie, Constraints on Archean trondhjemite genesis, *J. Geol.*, *100*, 57–68, 1992.

van Westrenen, W., J. Blundy, and B. Wood, Crystal-chemical controls on trace element partitioning between garnet and anhydrous silicate melt, *Am. Mineral.*, *84*, 838–847, 1999.

von Huene, R., and D. W. Scholl, Observations at convergent margins concerning sediment subduction, subduction erosion, and the growth of continental crust, *Rev. Geophys.*, *29*(3), 279–316, 1991.

Williams, W. C., Magmatic and structural controls on mineralization in the Paleocene magmatic arc between 22°40′ and 23°45′S, Antofagasta, II Region, Chile, Ph D. thesis, 182 pp., Univ. of Arizona, Tuscon, 1992.

Wörner, G., R. S. Harmon, J. Davidson, W. Moorbath, D. L. Turner, N. McMillan, C. Nye, Lopez-Escobar, and H. Moreno, The Nevados de Payachata volcanic region (18°S/69°W, N. Chile), 1, Geological, geochemical and isotopic observations, *Bull. Volcanol.*, *50*, 287–303, 1988.

Wörner, G., S. Moorbath, and R. S. Harmon, Andean Cenozoic volcanic centres reflect basement isotopic domains, *Geology*, *20*, 1103–1106, 1992.

Wörner, G., S. Moorbath, S. Horn, J. Entenmann, R. S. Harmon, J. P. Davidson, and Lopez-Escobar, Large- and fine-scale geochemical variations along the Andean arc of northern Chile (17.5–22°S), in *Tectonics of the Southern Central Andes*, edited by K.-J. Reutter, E. Scheuber, and P. Wigger, pp. 69–76, Springer-Verlag, New York, 1994.

A. Günther and E. Scheuber, Insitut für Geologie, Geophysik und Geoinformatik, Freie Universität Berlin, Malteserstrasse 74–100, D-12249 Berlin, Germany. (scheuber@geophysik.fu-berlin.de)

M. Haschke, Institut für Geowissenschaften, Universität Potsdam, Karl-Liebknecht-Strasse 24, D-14476 Potsdam, Germany. (mrh@geo.uni-potsdam.de)

W. Siebel, Institut für Mineralogie, Petrologie und Geochemie, Universität Tübingen, Wihelmstrasse 7, D-72074 Tübingen, Germany.